Journal of Medicinal Chemistry

Article

pubs.acs.org/jmc

Chemical Optimization of New Ligands of the Low-Density Lipoprotein Receptor as Potential Vectors for Central Nervous System Targeting

Jean-Daniel Malcor,[†] Nadine Payrot,[†,‡] Marion David,[‡] Aude Faucon,[‡] Karima Abouzid,[‡] Guillaume Jacquot,[‡] Nicolas Floquet,[†] Franck Debarbieux,[§,⊥] Geneviève Rougon,[§,⊥] Jean Martinez,[†] Michel Khrestchatisky,[∥,¶] Patrick Vlieghe,[‡] and Vincent Lisowski*[,†]

[†]Institut des Biomolécules Max-Mousseron, UMR5247 CNRS, UFR des Sciences Pharmaceutiques et Biologiques, Universités Montpellier I et II, 15 Avenue Charles Flahault, 34093 Montpellier Cedex 5, France

[‡]VECT-HORUS S.A.S., Faculté de Médecine Secteur Nord, CS80011, Boulevard Pierre Dramard, 13344 Marseille Cedex 15, France

[§]Aix-Marseille Univ, UMR6216, Institut de Biologie du Développement de Marseille Luminy, 13288 Marseille Cedex 9, France

[⊥]CNRS, UMR6216, Institut de Biologie du Développement de Marseille Luminy, 13288 Marseille Cedex 9, France

[∥]Aix-Marseille Univ, UMR7259, Laboratoire NICN, Faculté de Médecine Secteur Nord, 13344 Marseille Cedex 15, France

[¶]CNRS, UMR7259, Laboratoire NICN, Faculté de Médecine Secteur Nord, 13344 Marseille Cedex 15, France

Supporting Information

ABSTRACT: Drug delivery to the central nervous system is hindered by the presence of physiological barriers such as the blood–brain barrier. To accomplish the task of nutrient transport, the brain endothelium is endowed with various transport systems, including receptor-mediated transcytosis (RMT). This system can be used to shuttle therapeutics into the central nervous system (CNS) in a noninvasive manner. Therefore, the low-density lipoprotein receptor (LDLR) is a relevant target for delivering drugs. From an initial phage display biopanning, a series of peptide ligands for the LDLR was optimized leading to size reduction and improved receptor binding affinity with the identification of peptide **22** and its analogues. Further real-time biphoton microscopy experiments on living mice demonstrated the ability of peptide **22** to efficiently and quickly cross CNS physiological barriers. This validation of peptide **22** led us to explore its binding on the extracellular LDLR domain from an NMR-oriented structural study and docking experiments.

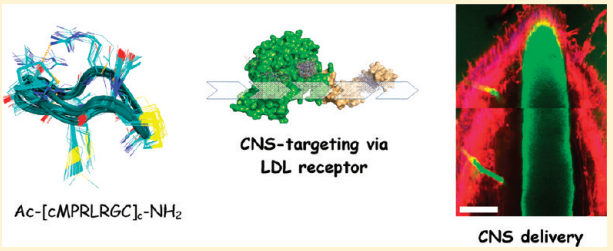

INTRODUCTION

The therapeutic area of central nervous system (CNS) disorders and diseases belongs to the most important segments of the worldwide pharmaceutical market along with cardiovascular and oncology. Currently, the CNS global market segment still remains underdeveloped and therapeutic options are mainly limited to chronic pain, insomnia, epilepsy, and affective disorders such as depression and schizophrenia.[1−3] One of the main drawbacks of targeting the CNS is that the delivery of drugs to the brain is hindered by the presence of physiological barriers such as the blood–brain barrier (BBB), the blood–cerebrospinal fluid barrier, the arachnoid epithelial membrane, and the blood–spinal cord barrier (BSCB). Like the BBB, the BSCB is another endothelial cell barrier that is reinforced by astrocytes, pericytes, and extracellular matrix. These barriers keep the CNS separated from the bloodstream by a highly impermeable endothelial cell network.[4−6] To overcome this major impediment, medicinal chemists developed drugs as small organic molecules with high lipid solubility and low molecular weight according to Lipinski's rule of five.[7,8] However, many serious CNS diseases such as Alzheimer's disease, brain/spinal cord injury, stroke, cancer, and HIV infection do not respond to such molecules, many of them exhibiting insufficient transcellular passive diffusion.[5,6,9] Most of these CNS disorders might be treated with large molecule drugs including peptides and proteins (antibodies, enzymes, cytokines, ...) which do not respond to Lipinski's rule of five. Such candidates have a great pharmacological potential but only a few efficiently cross the BBB or the BSCB.[10,11] In this context and considering the productivity crisis in pharmaceutical R&D,[12,13] development of new strategies able to deliver these molecules to the brain is challenging for modern drug discovery. Apart from passive diffusion (nonenergy requiring) or facilitated diffusion (energy or nonenergy requiring), active transport (energy requiring) systems such as receptor-mediated transcytosis (RMT) is one serious option for BBB or BSCB targeting and delivery of drugs to the CNS.[14]

RMT is an active physiological process involved in the task of nutrient transport for brain homeostasis. It may also be used to shuttle therapeutics into the CNS through a noninvasive manner. RMT employs the vesicular trafficking machinery and

Received: November 4, 2011
Published: January 18, 2012

dx.doi.org/10.1021/jm2014919 | *J. Med. Chem.* 2012, 55, 2227−2241

occurs in three steps: receptor-mediated endocytosis at the luminal side, transfer through the cytoplasm into vesicles, and exocytosis of the nutrient and/or drug at the abluminal side of the brain capillary endothelium. The most important aspect in the design of vector−drug conjugates for BBB or BSCB targeting is clearly the choice of the CNS vector and its cognate receptor. Currently, several RMT systems are known to be localized on the BBB and the BSCB including the transferrin receptor (TfR), the insulin receptor (INSR), the insulin-like growth factor receptor (IGFR), the leptin receptor (LEPR), the low-density lipoprotein receptor (LDLR), the low-density lipoprotein receptor-related proteins (LRP), the scavenger receptors class A type I (SR-AI or SCARA1) and class B type I (SR-BI or SCARB1), and the diphtheria toxin receptor.[5,15,16] There have been significant recent developments in the area of RMT-based brain drug delivery achieved by using endogenous ligands,[17] antibodies,[18] brain-targeted nanoparticles,[19,20] or peptides[21,22] as CNS vectors targeting such receptors.

The LDLR family is such a group of cell surface endocytic receptors. The nine members of this family include the LDL receptor (LDLR), the LRP1, a closely related receptor termed LRP1b, the megalin (gp330 or LRP2) receptor, the very-low-density lipoprotein receptor (VLDLR), the apolipoprotein E receptor 2 (ApoER2 or LRP8), the sortilin-related receptor with A type repeats (sorLA/LR11), the multiple epidermal growth factor-like domain 7 (MEGF7 or LRP4), and the LRP5/6. Not only are these receptors mediators of cholesterol uptake/metabolism but also allow the internalization and the degradation of multiple ligands involved in diverse metabolic pathways.[23−25] Recent studies have suggested that the LDL receptors are involved in endocytosis of drugs (aminoglycosides, cyclosporine A) and lipid-based formulations, and new results in the LRP members have shown that LDL receptors are relevant targets to design vectors in the field of RMT-based drug transport into the brain.[24,26−28] As part of a research program for novel ligands of endocytic receptors, a phage display biopanning directed to the extracellular domain of the human LDLR (hLDLR) led to the identification of a family of cyclic peptide inserts with a MPR-consensus/conserved central motif. One of these candidates, the 15-mer cyclic peptide **1** (Figure 1), was selected for its ability to bind the hLDLR and to cross endothelial cells both in vitro and in situ.[29] Here, with the aim of exploring structure−affinity relationship (SAR) and developing novel analogues of peptide **1** with higher binding affinity for the hLDLR, we performed a series of medicinal-chemistry-based structural modifications. Binding affinity of the neo-synthesized analogues was evaluated using a high efficiency FRET assay. In addition, plasma stability properties of these analogues were assessed. Real time biphoton microscopy in the spinal cord of living mice of Rhodamine Red-X conjugated to one of the most potent vector derivatives provided evidence of its in vivo CNS-targeting and its BSCB-crossing properties.

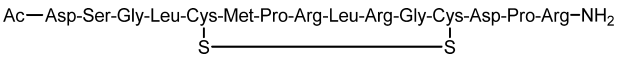

Figure 1. Structure of peptide **1**.

RESULTS AND DISCUSSION

The identification of the cyclic hit peptide **1** led us to explore its chemical optimization in order to afford more druglike candidates as potential CNS vectors. All derivatives of peptide **1** were first evaluated in vitro by a FRET assay for their potential to displace the S-tagged reference peptide **1** bound to CHO cells expressing hLDLR fused to the red fluorescent protein DsRed2 (CHO-hLDLR-DsRed2 cells). The detected fluorescence is directly related to the amount of S-Tag bound to cells. First, our goal was to determine the minimal active sequence, i.e., with conserved hLDLR-binding affinity, and the role of the disulfide bridge before investigating plasma stability properties. As part of a SAR study, such modifications included (i) initial alanine- and D-scanning (i.e., Ala-scan and D-scan, respectively), (ii) disulfide bridge changes, (iii) substitution of natural amino acids by non-natural residues, and (iv) synthesis of pseudo-peptides (i.e. introduction of pseudo-peptide bonds).

As a preliminary test to explore disulfide bridge influence, the in vitro affinity of the linear form of peptide **1** was assessed (50% displacement of the S-tagged reference peptide **1**) which demonstrated a conserved binding affinity for hLDLR. Although unexpected, this result could be explained by the spontaneously re-formation of the disulfide bridge in the conditions used in the FRET assay. Therefore, a linear analogue of peptide **1** was synthesized by replacing each cysteine by a serine, which led to a complete loss of binding affinity, pointing to the key role of the two cysteines in the binding to the hLDLR (Table 1, compounds **2** and **3**).

Ala-Scan and Truncation. The first step toward chemical optimization of peptide **1** consisted of replacing each amino acid by an alanine residue in order to identify which residues are required for binding to the LDLR. Results of the in vitro binding assays showed that the central pattern of peptide **1**, made out of Cys_5, Met_6, Pro_7, Arg_8, Arg_{10}, Cys_{12}, and to a lesser extent Leu_9 and Gly_{11} (Table 1, compounds **8**−**15**), was required to retain good affinity. This confirmed the importance of the disulfide bridge and the Met-Pro-Arg pattern found in many peptide sequences identified from the phages selected on CHO cells overexpressing the hLDLR (i.e., biopanning). As the other residues on either part of the cysteines seemed to be of less significance (Table 1, compounds **4**−**7**, **16**−**18**), the N-terminal and C-terminal extracyclic ends were first removed. The central pattern alone exhibited a better binding affinity for the hLDLR than the original peptide **1**, thus reducing the minimal active sequence 2-fold. Further attempts to lower the number of amino acids remained unsuccessful (Table 1, compounds **19**−**21**). An Ala-scan carried out on this shorter peptide **19** confirmed that Cys, Arg, Met, and Pro remain essential for binding.[30]

D-Scan. The influence of the side chain orientation of each residue was investigated by carrying out a D-scan on peptide **19**. Such experiments might allow incorporation of non-natural amino acids in the sequence, making the peptides less sensitive to endogenous proteases, a major issue with peptide-based therapeutics.[10] Each amino acid was thus replaced by its D-enantiomer (except for Gly). Natural configuration was required for the Met_2-Pro_3-Arg_4 pattern, Arg_6, and to a lesser extent Leu_5 and Cys_8. On the contrary, substitution of Cys_1 by a D-Cys led to a significant increase of hLDLR-binding affinity as a consequence of a conformational rearrangement of the peptidic backbone (Table 1, compounds **22**−**28**). These results indicate that even a local change in the topology of the peptide has a drastic effect on the binding to the receptor, highlighting the tight correlation between the structure of the peptide and its receptor affinity. Moreover, these promising results enabled us to introduce a non-natural amino acid, which in turn may increase the plasma stability of our compounds. All further in vitro binding assays

Table 1. SAR Study from Peptide 1

compd	sequence	% displacement[a]	compd	sequence	% displacement[a]
1	Ac-DSGL[CMPRLRGC]$_c$DPR-NH_2	55	**23**	Ac-[CmPRLRGC]$_c$-NH_2	0
2	Ac-DSGLCMPRLRGCDPR-NH_2	50	**24**	Ac-[CMpRLRGC]$_c$-NH_2	0
3	Ac-DSGLSMPRLRGSDPR-NH_2	0	**25**	Ac-[CMPrLRGC]$_c$-NH_2	0
4	Ac-ASGL[CMPRLRGC]$_c$DPR-NH_2	55	**26**	Ac-[CMPRlRGC]$_c$-NH_2	40
5	Ac-DAGL[CMPRLRGC]$_c$DPR-NH_2	20	**27**	Ac-[CMPRLrGC]$_c$-NH_2	0
6	Ac-DSAL[CMPRLRGC]$_c$DPR-NH_2	58	**28**	Ac-[CMPRLRGc]$_c$-NH_2	40
7	Ac-DSGA[CMPRLRGC]$_c$DPR-NH_2	64	**29**	Ac-[CGRLRPMc]$_c$-NH_2	0
8	Ac-DSGLAMPRLRGCDPR-NH_2	0	**30**	Ac-[CmprlrGc]$_c$-NH_2	0
9	Ac-DSGL[CAPRLRGC]$_c$DPR-NH_2	0	**31**	Ac-[cGrlrpmC]$_c$-NH_2	0
10	Ac-DSGL[CMARLRGC]$_c$DPR-NH_2	3	**32**	Ac-M[cPRLRGC]$_c$-NH_2	28
11	Ac-DSGL[CMPALRGC]$_c$DPR-NH_2	0	**33**	Ac-MP[cRLRGC]$_c$-NH_2	34
12	Ac-DSGL[CMPRARGC]$_c$DPR-NH_2	35	**34**	Ac-MPR[cLRGC]$_c$-NH_2	34
13	Ac-DSGL[CMPRLAGC]$_c$DPR-NH_2	2	**35**	amide bridge	12
14	Ac-DSGL[CMPRLRAC]$_c$DPR-NH_2	20	**36**	lanthionine bridge	41
15	Ac-DSGLCMPRLRGADPR-NH_2	0	**37**	alkene bridge	22
16	Ac-DSGL[CMPRLRGC]$_c$APR-NH_2	70	**38**	triazole bridge	13
17	Ac-DSGL[CMPRLRGC]$_c$DAR-NH_2	52	**39**	guanidinium bridge	0
18	Ac-DSGL[CMPRLRGC]$_c$DPA-NH_2	55	**79**	Ac-[c-ψ(CH_2-NH)-MPRLRGC]$_c$-NH_2	37
19	Ac-[CMPRLRGC]$_c$-NH_2	74	**80**	Ac-[cM-ψ(CH_2-NH)-PRLRGC]$_c$-NH_2	33
20	Ac-[CMPRC]$_c$-NH_2	0	**81**	Ac-[cMP-ψ(CH_2-NH)-RLRGC]$_c$-NH_2	0
21	Ac-[CMPRGC]$_c$-NH_2	39	**82**	Ac-[cMPR-ψ(CH_2-NH)-LRGC]$_c$-NH_2	58
22	Ac-[cMPRLRGC]$_c$-NH_2	100	**83**	Ac-[cMPRL-ψ(CH_2-NH)-RGC]$_c$-NH_2	40

[a]For compounds **1**–**28** (10 μM): % displacement of the S-tagged reference peptide **1** (10 μM) bound to CHO-hLDLR-DsRed2 cells. For compounds **29**–**39**, **79**–**83** (10 μM): % displacement of the S-tagged reference peptide **22** (10 μM) bound to CHO-hLDLR-DsRed2 cells.

were carried out with compound **22** as the reference peptide (displacement of the S-tagged reference peptide **22** is therefore set to 50%). Retro, inverso, and retro–inverso derivatives were also synthesized, as they often have similar interesting properties but higher plasma stability than the parent peptide. However, none of those modifications could retain binding affinity for the hLDLR (Table 1, compounds **29**–**31**). In our case, this is not surprising and is in agreement with the D-scan experiments.

Disulfide Bridge Modification. Although the disulfide bridge seems essential for binding to the hLDLR, it may be a metabolically and chemically unstable bond under reducing conditions by thiol-containing molecules (e.g., glutathione or serum albumin).[31] Replacement of the S–S bond by more stable alternatives, such as amide bond, thioether linkage, carbon–carbon double bond, triazole or guanidinium moieties, has long been regarded as an attractive strategy to overcome this particular problem of instability but also to introduce additional constraints to a peptide.[32−35] Such bridge-induced structural preorganization generally reduces the two major limitations of peptide-based therapeutics, proteolysis, and lack of receptor selectivity. Therefore, exploring peptide constraints is often a fruitful approach for the improvement of receptor-specific ligands.[36]

First of all, in our SAR study, the ring size of the disulfide bridge was reduced by shifting gradually D-Cys_1 on the N-terminus side toward the C-terminus end. However, this resulted in a loss of affinity for each attempt (Table 1, compounds **32**–**34**).

1. Amide Bridge. The most common strategy to synthesize a cyclic peptide is to create an amide bond. In order to maintain the same ring size as the reference peptide **22**, the two cysteines were replaced by a D-diaminopropionic residue (D-Dap(Alloc)) on the N-terminus and by an Asp(OAll) residue on the C-terminus. Following assembly of linear peptide on the Rink amide resin and acetylation of the N-terminus using Ac_2O in DCM, both Alloc and allyl protections were simultaneously removed with tetrakis(triphenylphosphine)palladium(0) (0.25 equiv) and phenylsilane (24 equiv) in DCM. The subsequent cyclization was carried out by coupling the amine on the D-Dap side chain with the carboxylic acid of the Asp side chain. This on-resin coupling was performed in NMP using HBTU (6 equiv) and HOBt (6 equiv) as coupling agents and NMM (12 equiv) as base. A negative TNBS test indicates that the reaction took place before cleavage with a TFA/TIS/H_2O/EDT mixture (Scheme 1).

2. Lanthionine Bridge. Another straightforward disulfide bridge modification is the removal of a sulfur atom, leading to the more constrained lanthionine bridge (i.e., thioether linkage). The cyclic peptide **22** with a disulfide bridge was first synthesized using standard Fmoc peptide chemistry followed by DMSO oxidation in solution. It was then stirred overnight at room temperature in TEA/H_2O (9:1). The mechanism leading to the lanthionine bridge in basic conditions is thought to involve the

Scheme 1. Formation of the Amide Bridge

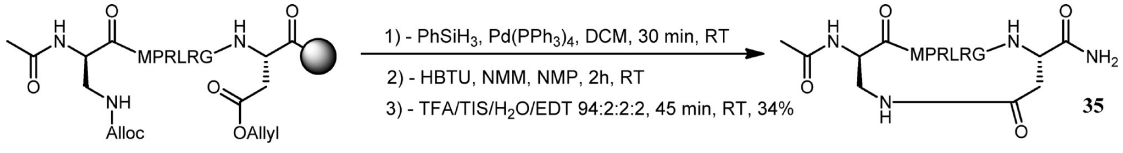

dx.doi.org/10.1021/jm2014919 | J. Med. Chem. 2012, 55, 2227–2241

Scheme 2. Proposed Mechanism for the Synthesis of Lanthionine

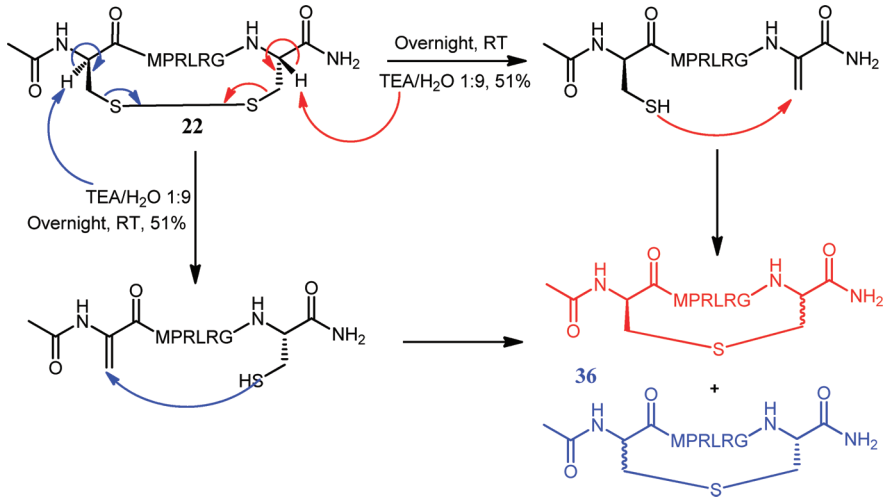

Scheme 3. Synthesis of the Alkene Bridge

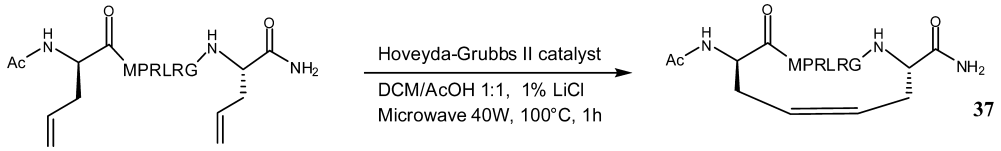

Scheme 4. Synthesis of the 1,2,3-Triazole Bridge

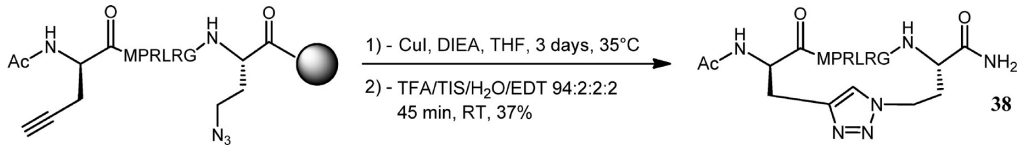

elimination of one of the two thiol moieties followed by the attack of the second thiol on the newly formed dehydroalanine residue (Scheme 2).[37] This implies a loss of stereochemistry on the α carbon of one of the two cysteines. A mixture of four isomers is thus obtained which could not be easily separated.

3. Alkene Bridge. A more recent approach to side chain cyclization uses the chemospecific linkage of olefin-containing side chains through Grubbs ring closing metathesis (RCM).[38,39] This method led to the dicarba analogue of peptide **22**. The linear precursor was prepared by standard supported Fmoc peptide chemistry on Rink amide resin. D-Allylglycine (D-Hag) was incorporated instead of D-Cys_1 and allylglycine (Hag) instead of Cys_8 in order to retain the size of the ring.[40] The RCM was performed in solution using the Hoveyda−Grubbs second generation ruthenium catalyst (15 mol %) in an AcOH/DCM mixture. LiCl was added in order to enhance the folding of the peptide by coordination with the amino acid side chains, therefore favoring intramolecular cyclization.[41] The experiment was carried out under microwave irradiation (40 W, 100 °C), thus reducing significantly the reaction time to only 1 h and achieving 100% conversion of the starting material (Scheme 3).

4. 1,2,3-Triazole Bridge. On the basis of recent "click chemistry" developments,[42,43] another analogue cyclized by a 1,2,3-triazole moiety was also synthesized by using Huisgen 1,3-dipolar cycloaddition in the presence of a base and a copper(I) species.[44] D-Cys_1 and Cys_8 were replaced by D-propargylglycine (D-Pra) and 4-azido-(*S*)-homoalanine (Aha), respectively. Cyclization was then carried out on solid support in THF at 35 °C for 3 days with DIEA (10 equiv) and copper iodine (2 equiv) as catalyst.[45] The final product was obtained after standard acidic cleavage from the resin (Scheme 4).

5. Guanidinium Bridge. We have recently described a new methodology to generate cyclic peptides with unusual guanidinium bridges.[46] Moreover, guanidinium moieties carried by the arginine residues were proven to play a key role in the binding affinity for the LDLR. This prompted us to synthesize such a derivative of peptide **22**. This was achieved by starting with the replacement of D-Cys_1 and Cys_8 in peptide **22** by D-Dap(Alloc) and Dap(Mtt), respectively. The next step was to remove the Alloc protection on the D-Dap in position 1 using tetrakis(triphenylphosphine)-palladium(0) (0.2 equiv) and phenylsilane (24 equiv) in DCM. Then an isothiocyanate moiety was introduced by reaction of the free amine with di-2-pyridyl thionocarbonate (5 equiv) in DCM. After removal of the Mtt group located on the Dap in position 8 with DCM/TFE/AcOH (7:2:1), cyclization occurred in THF at reflux in the presence of TEA (4 equiv) to give the cyclic thiourea in slightly basic conditions. The subsequent S-methylation was performed by treatment of the resin with a solution of 0.2 M methyl iodide in DMF. Heating the resin in DMSO at 80 °C for 12 h in the presence of 2 M ammonium acetate eventually led to the cyclic peptide containing a guanidinium bridge. The final product was obtained after cleavage from the resin with a TFA/TIS/H_2O/EDT mixture (Scheme 5).

6. Results for Modified-Bridge Analogues. In vitro binding assays showed once again that the affinity was closely linked to the structure of the peptide. The amide **35**, alkene **37**, and

dx.doi.org/10.1021/jm2014919 | *J. Med. Chem.* 2012, 55, 2227−2241

Scheme 5. Synthetic Route for the Formation of the Guanidinium Bridge

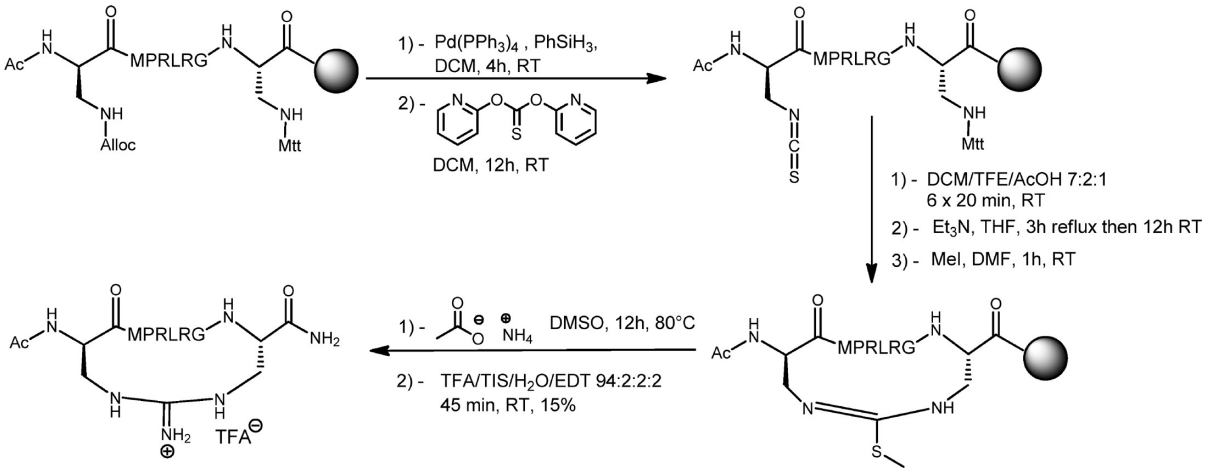

triazole **38** bridges all resulted in compounds with lower binding affinity for the hLDLR. The guanidinium bridge **39** led to a complete loss of affinity maybe because of the positive charge, even though basic residues Arg_4 and Arg_6 seemed to be essential for binding. On the contrary, the lanthionine derivative **36** only had a small effect on affinity, despite the fact that it introduces a greater constraint to the peptide. This also suggested that sulfur atoms of cysteine residues might be involved in the binding to the hLDLR (Table 1, compounds **35**–**39**).

Amino Acid Substitution. Our initial screening showed the significance of each residue and the importance of the cyclic backbone for this family of peptides. However, except for D-Cys_1, all amino acids are natural, making the peptide especially vulnerable to proteases found in the bloodstream.[10] To overcome this major issue and to increase the binding affinity for the LDLR, residues on peptide **22** were replaced by various non-natural analogues (see Supporting Information for structures).

1. Substitution of Cysteine(s). The two cysteines on either end of peptide **22** are key residues because of their ability to form a disulfide bridge, awarding the peptide with crucial structural constraint, as indicated by Ala-scan and disulfide bridge modification results. Our goal here was to study the influence of a more constrained bridge by replacing the cysteine residue(s) by penicillamine (Pen) residue(s). Eight derivatives exploring all the possibilities of swapping the two Cys by Pen and/or D-Pen were synthesized (Table 2, compounds **40**, **41**, and **43**–**48**). In vitro tests showed that replacing D-Cys_1 by a penicillamine residue (Pen or D-Pen) increased the binding affinity for the targeted receptor, regardless of the configuration. Indeed, up to 65% of the reference S-tagged peptide **22** could be displaced in the in vitro test (**40** and **41**). However, only the substitution of Cys_8 by Pen was tolerated to retain affinity (**43** vs **44**) and any association of two Pen residues in the same peptide was deleterious (**45**–**48**). Finally, mercaptopropionic acid (Mpa) was coupled to the N-terminus side of the peptide in position 1, but this modification caused a slight decrease of affinity (**42**). Altogether, these results confirmed our assumption that conformational structure of the peptide was crucial for its binding to the hLDLR.

2. Substitution of Methionine. Our initial Ala-scan carried out on peptide **1** showed that methionine was essential for binding to hLDLR. Surprisingly, its substitution by the nonoxidable isostere norleucine (Nle) resulted in a complete loss of affinity in the preliminary study of peptide **1** (data not shown), which indicated that the sulfur atom was essential for binding affinity. This result was later confirmed by the introduction of methylated homoserine (HSer(OMe)) as oxygen-derived isostere or oxidized methionine (Met(O)) in position 2 of peptide **22** instead of methionine (Table 2, compounds **49** and **50**). Attempts to constrain the side chain bearing the sulfur atom with the use of thiazolidine-4-carboxylic acid (Thz) and 3-(2-thienyl)-(*S*)-alanine (Thi) residues were also unsuccessful (Table 2, compounds **51** and **52**).

3. Substitution of Proline. As previously observed, the structure of the peptide has a crucial role for binding to the target receptor. Proline, which is known to induce cis/trans isomerization,[47] probably plays an important role in this structure, as suggested by the results of the Ala-scan on peptide **1**. Several modifications involving the Pro_3 residue were thus carried out in order to modify the structural constraints, including the introduction of the more polar 4-hydroxyproline (Hyp), the acyclic sarcosine (Sar), the six-membered pipecolic acid (Pip), the bicyclic 1,2,3,4-tetrahydroisoquinoline-1-carboxylic acid (Tic), the thiazolidine-4-carboxylic acid (Thz), and the β-analogue aminobenzoic acid (Abz) (Table 2, compounds **53**–**58**). Although most of the attempts resulted in a decreased affinity (**53**, **54**, **56**, **58**), addition of one more sulfur atom by the use of Thz (**57**) produced an 88% displacement of the S-tagged reference peptide **22**. This promising result led us to pursue optimization with the association of Pen residue in position 1. With Pen (**59**), a good affinity was maintained. However, with D-Pen (**60**), we observed a 91% displacement of the reference peptide. The use of Pip (**55**) also had some interesting properties (75% displacement of the reference peptide). We therefore synthesized Pip-containing peptides along with D-Cys_1 substituted by Pen (**61**) or D-Pen (**62**). These peptide derivatives showed a slight increase in binding affinity for the hLDLR (with displacements of the reference peptide up to 75%).

4. Substitution of Arginine. Arginine substitution is an interesting aspect to explore, since both residues are essential to proper binding and bear a guanidine moiety with specific basic properties. However, changing Arg_4 and Arg_6 with other amino acids bearing basic moieties on the side chain, such as lysine[48] or ornithine (Orn), decreased the affinity (**63**–**65**). Additional modifications on the guanidine moiety with introduction of $Arg(NO_2)$ or citrulline (Cit) were also unsuccessful (**66**–**67**,

dx.doi.org/10.1021/jm2014919 | J. Med. Chem. 2012, 55, 2227–2241

Table 2. Analogues of Peptide 22 and Percentage Displacement of the S-Tagged Reference Peptide 22

compd	D-Cys$_1$	Met$_2$	Pro$_3$	Arg$_4$	Leu$_5$	Arg$_6$	Gly$_7$	Cys$_8$	% displacement[a]
22									50
40	D-Pen								65
41	Pen								62
42	Mpa								31
43								Pen	52
44								D-Pen	0
45	D-Pen							Pen	3
46	Pen							D-Pen	0
47	D-Pen							D-Pen	9
48	Pen							Pen	9
49		HSer(OMe)							0
50		Met(O)							0
51		Thz							0
52		Thi							0
53			Hyp						0
54			Sar						22
55			Pip						75
56			Tic						21
57			Thz						88
58			Abz						0
59	Pen		Thz						77
60	D-Pen		Thz						91
61	Pen		Pip						75
62	D-Pen		Pip						70
63				Orn					28
64						Orn			0
65				Orn		Orn			31
66				Cit					9
67				Arg(NO$_2$)					17
68				homoArg					22
69				Agb					23
70				Agp					8
71						Cit			0
72						Arg(NO$_2$)			0
73						homoArg			11
74							Sar		46
75							D-Ala		54
76			Thz				Sar		74
77	Pen		Thz				Sar		80
78	D-Pen		Thz				Sar		84

[a]% displacement of the S-tagged reference-peptide **22** (10 μM) bound to CHO-hLDLR-DsRed2 cells.

72, **73**). We then studied the influence of the length of the side chain by adding one carbon atom (HomoArg) to the side chain and by removing one or two carbon atoms (Agb and Agp, respectively) from the side chain. The results were once again unsuccessful on both arginine substitutions (**68**–**70** and **73**).

5. Substitution of Glycine. Although replacing glycine by alanine during the Ala-scan of peptide **1** did not have any significant influence on the affinity, it is known that glycine might play a role in the structure of the peptide because of its flexibility. We tried to add structural constraints by introducing D-alanine or sarcosine (Sar) instead of glycine. In these cases, the binding affinity for hLDLR was maintained (**74** and **75**). We then introduced Sar in the best Thz-containing sequences (**76**–**78**), as Thz proved to be useful earlier on. Then again, binding affinity was maintained but was not improved compared to the peptide containing glycine (**57**, **59**, **60**). It might nevertheless be useful to replace glycine with Sar, as it adds a non-natural amino acid within the sequence, which might lead to analogues with lower susceptibility to proteolytic degradation (Table 3).

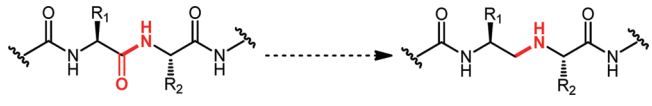

Figure 2. Analogy between a regular peptide bond and a reduced peptide bond.

Reduction of Peptide Bonds. Another widely spread technique to increase plasma stability of a peptide is to modify one or more of its peptide bonds. The aim was to substitute the amide bond by a surrogate with a similar structure but less sensitive to endogenous enzymes. In this case, the peptide bond between various residues was replaced by a reduced bond, where the carbonyl moiety was removed (Figure 2).[49] Features provided by this amide bond isostere included increased flexibility, resistance

dx.doi.org/10.1021/jm2014919 | J. Med. Chem. 2012, 55, 2227–2241

Table 3. Estimated First-Order Degradation Parameters of Peptide 22 and Some of Its Analogues in Freshly Collected Swiss Mouse Blood at 37 °C

compd	sequence	k (h^{-1})[a]	$t_{1/2}$ (h)[b]
19	Ac-[CMPRLRGC]$_c$-NH_2	0.472	1.47
22	Ac-[cMPRLRGC]$_c$-NH_2	0.242	3.03
57	Ac-[cM″Thz″RLRGC]$_c$-NH_2	0.385	1.80
61	Ac-[L-PenM″Pip″RLRGC]$_c$-NH_2	0.407	1.70
62	Ac-[D-PenM″Pip″RLRGC]$_c$-NH_2	0.236	2.99
76	Ac-[cM″Thz″RLR″Sar″C]$_c$-NH_2	0.306	2.26
78	Ac-[D-PenM″Thz″RLR″Sar″C]$_c$-NH_2	0.239	2.90

[a] k (degradation rate constant) is estimated from individual exponential regression curves given by $C(t) = C_0e^{-kt}$. [b] Half-lives are given by $t_{1/2} = \ln 2/k$.

to enzymatic degradation, and introduction of a protonation site under physiological conditions.[50−53]

Its incorporation into the peptide sequence required the synthesis of the Weinreb amide derivative obtained by coupling the Weinreb amine (3 equiv) with the appropriate Fmoc-amino acid in standard coupling conditions, with DIEA (4 equiv) as the base and BOP (3 equiv) as the activating agent.[54] The subsequent reduction was performed using lithium aluminum hydride (6 equiv) in THF without further purification of the Weinreb amine. The aldehyde was an unstable intermediate,[55] which was condensed immediately to the growing peptide chain by reductive amination, on solid support under nitrogen with sodium cyanoborohydride (8 equiv) as a reductive agent in anhydrous DMF containing 1% acetic acid. Finally, the target peptides were obtained after standard SPPS followed by acidic cleavage and cyclization in the conditions previously described (Scheme 6).

In our SAR study on peptide **22**, introduction of a reduced bond generally resulted in a decrease of binding affinity for hLDLR. However, a reduced bond between Arg_4 and Leu_5 did not have a negative effect on binding affinity of the peptide for the hLDLR. As an example, this result was of particular interest regarding trypsin-like proteases able to cleave Arg-containing peptide bonds (Table 1, compounds **79**−**83**).

Plasma Stability Study. We compared the in vitro plasma stability of the minimal active sequence, namely, peptide **19** (all natural amino acids), with that of some analogues (**22**, **57**, **61**, **62**, **76**, and **78**). These analogues were chosen because of their higher binding affinity for hLDLR when compared to peptide **19** and because they harbored the most relevant combinations of non-natural amino acids at positions 1, 3, and 7. The in vitro plasma stability was assessed using a liquid chromatography−tandem mass spectrometry (LC−MS/MS) analytical method. As reported in Table 3, peptide **19** showed an in vitro half-life ($t_{1/2}$) of 1.47 h when incubated in freshly collected Swiss mouse blood at 37 °C. Interestingly, all the studied analogues of peptide **19**, comprising non-natural amino acids, showed higher plasma stability. Regarding the nature of amino acid at position 1, the comparison between peptides **19** and **22** demonstrated that substitution of the L-Cys by its non-natural D-enantiomer resulted in a near 2-fold improvement in plasma stability. This observation was further confirmed when comparing peptides **61** and **62** where the D-Cys_1 residue was substituted by D- and L-Pen, respectively. In contrast the nature of the D-amino acid at position 1 had no clear impact on plasma stability (peptides **76** vs **78**). With regard to the amino acid at position 3, a comparison between peptides **22** and **57** demonstrated that substitution of Pro by Thz resulted in a near 2-fold decrease in plasma stability. Finally, substitution of Gly by Sar at position 7 increased moderately the plasma stability (peptides **57** vs **76**). Taken together, compounds **22**, **62**, and **78** elicited the highest plasma stability within this series, namely, ∼3 h.

NMR-Oriented Structural Study on Peptide 22 and Docking Experiments. The results of our SAR study convinced us that a tight correlation exists between the conformational constrained peptides and their binding affinity for the hLDLR. This prompted us to perform first a preliminary NMR-based structural analysis to grasp the conformational pattern of peptide **22** and to further specify its binding domain on the hLDLR. Indeed, the extracellular part of this receptor encompasses several functional domains: the ligand binding domain, the EGF precursor homology domain, and the O-glycosylation rich domain. In order to determine which of these domains binds the peptide **22**, "minireceptors", sequentially deleted of these domains, were expressed in transfected CHO cells. Results show that peptide **22** binds to the EGF precursor homology domain and not to the natural ligand binding domain (data not shown). These observations prompted us to perform docking experiments on the crystal structure of the extracellular hLDLR domain (structure available on the Protein Data Bank, PDB entry 3M0C) to identify putative binding regions for peptide **22**.

Among the set of 20 000 conformations generated for the peptide, only 133 conformers were found as fully respecting all the applied NOE constraints derived from NMR experiments. These conformers were highly related to each other as reported in Figure 3. Nevertheless, slightly different possible orientations of the main chain were noted, especially around the Pro3 residue. As a common feature to all these conformers, a β-turn spanned the Met-Pro-Arg-Leu residues. This turn was stabilized by an H-bond between the carbonyl group of Met2 and the amide proton of Leu5. Two other possible H-bonds were noted

Scheme 6. Synthetic Route for the Incorporation of a Reduced Peptide Bond

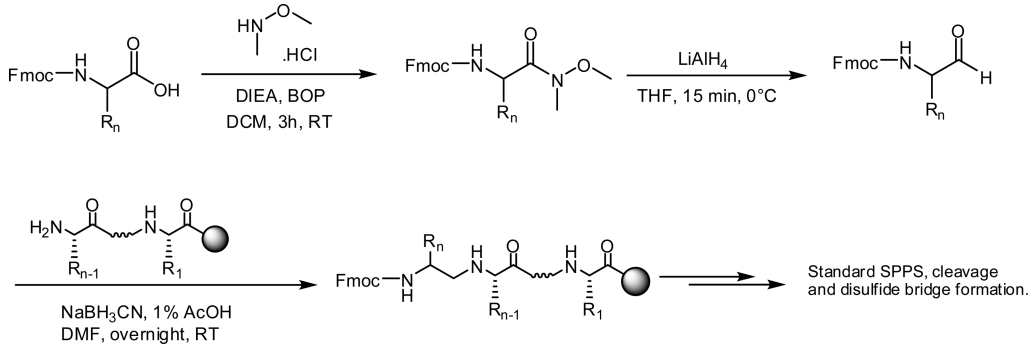

dx.doi.org/10.1021/jm2014919 | J. Med. Chem. 2012, 55, 2227−2241

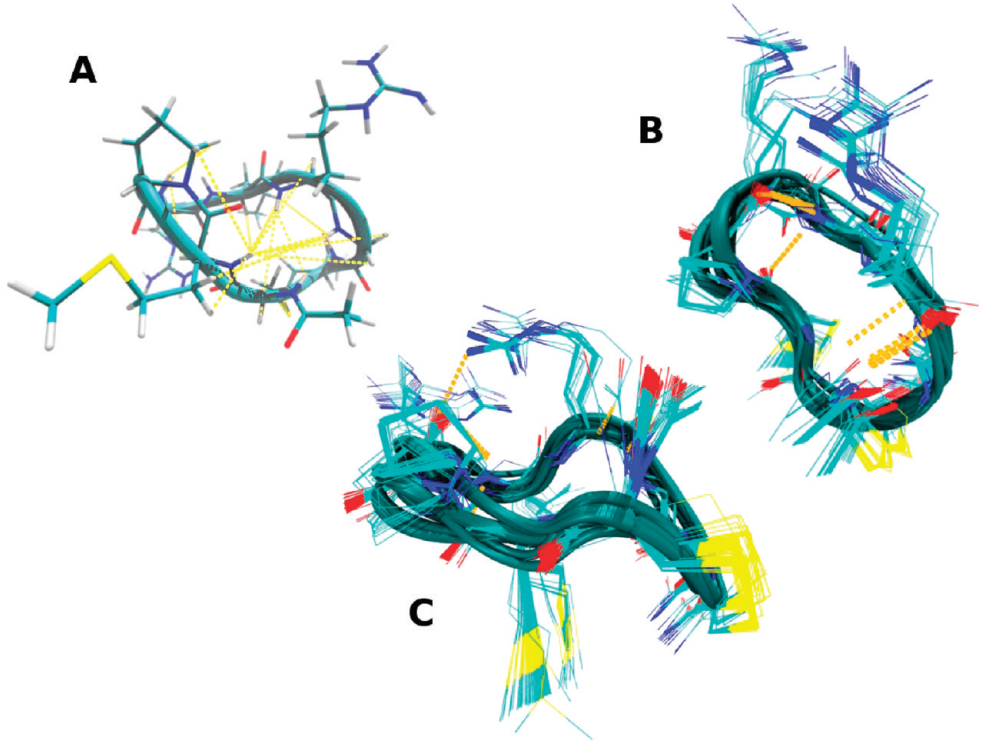

Figure 3. (A) Starting random conformation of the peptide with NOE constraints that were injected into the models as reported by yellow dashed lines. (B, C) Two different views of the 133 retained conformations of the peptide that fully respected the whole set of NOE constraints. On these models, hydrogen bonds are reported as orange lines.

in these models involving either the C═O of Pro3 with HN of Leu5 or the *N*-acetyl group of Cys1 with the C═O of Arg6. After clustering of the 133 conformers with PTRAJ, three representative conformations were selected for further docking experiments against the receptor (conf.1 to conf.3, Figure 4).

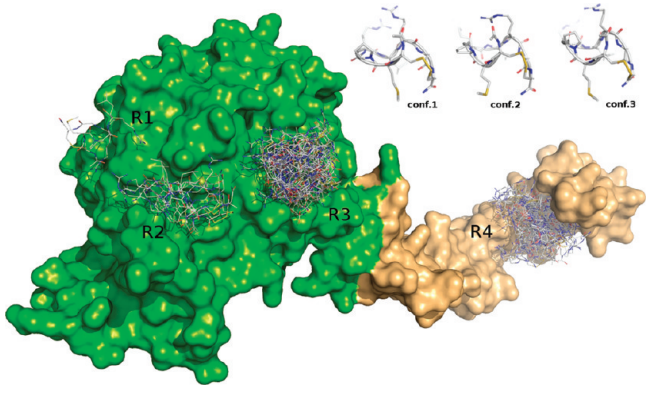

Figure 4. Results of the blind docking performed with VINA for the three representative conformers of the peptide (conf.1 to conf.3) against the PDB 3M0C structure. The docking was performed in two separate regions (green, orange) to minimize convergence problems. Four putative regions of binding were determined (noted as R1−R4).

A first docking was performed with VINA for each of these peptide conformers against the two green/orange regions as depicted in Figure 4. Interestingly, only four putative regions of binding were delimited by this first blind docking protocol further named as R1 (region 1), R2 (region 2), R3 (region 3), and R4 (region 4) (Figure 4). Three of these (R1−R3) were located on the β-barrel, whereas the last R4 region corresponded to the EGF like repeat domain A, close to a calcium binding site. To specify the possible binding modes of the peptide in each of these regions, additional docking calculations were performed with the Autodock software in a sphere radius of 15 Å around residues 533 (R1), 569 (R2), 555 (R3), and 313 (R4), respectively. The best poses obtained in each of these regions were reported in Figure 5. No important differences in binding energies were noted among the different regions even if a small preference was retrieved for regions R2 and R4 (predicted ΔG of binding of ∼1−6 μM vs 100−200 μM for regions R1 and R3). These values are in the range observed experimentally for the peptide **22**−receptor interaction.[56] The most important contacts established between the peptide and the protein surface were also reported in Figure 5 including residues Glu493 and Glu537 (R1), Asn570 and Asp568 (R2), Asp595, Glu594, and Asp548 (R3) or Glu316 (R4). Many other contacts were found in each of these models but involving atoms from the main chain of the protein (details not reported). These models should provide tracks for site-directed mutagenesis experiments on the key residues mentioned above, especially for regions R2 and R4.

Real Time Biphoton Microscopy on Living Mice. To validate the ability of peptide **22** to reach the CNS in living mice, imaging experiments were carried out by real time in vivo biphoton microscopy in the spinal cord. This imaging technique is, to date, the only noninvasive technique offering a submicrometer 3D optical resolution in thick samples of diffusing tissues. It is therefore valuable to study the biodistribution of pharmaceutics at high resolution. As only fluorescent objects can be detected, peptide **22** and a scrambled peptide of **22** as control were coupled to a fluorescent dye Rhodamine Red-X, a molecule that does not cross the BBB and the BSCB, prior to systemic injection in the animal. The fluorescent peptides were thus prepared according to the methodology described by Lefevre.[57]

dx.doi.org/10.1021/jm2014919 | *J. Med. Chem.* 2012, 55, 2227−2241

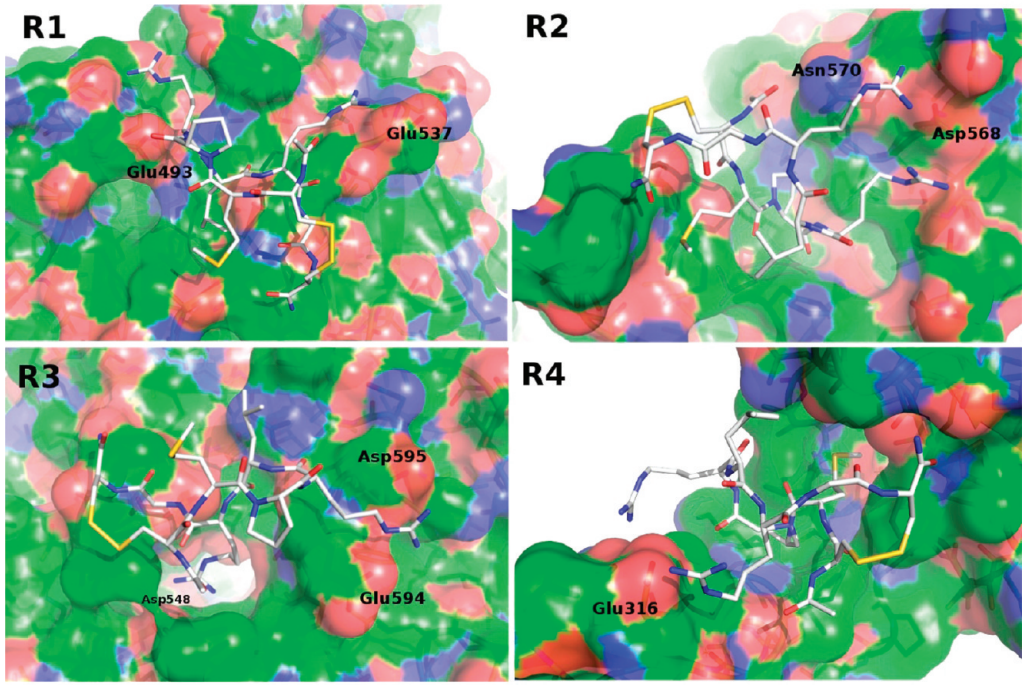

Figure 5. Best poses obtained with Autodock in each of the four regions R1, R2, R3, and R4 previously identified with VINA. The most important contacts were reported, especially involving the two arginines of the peptide.

Scheme 7. Synthetic Route for Fluorescent Probe of Peptide 22

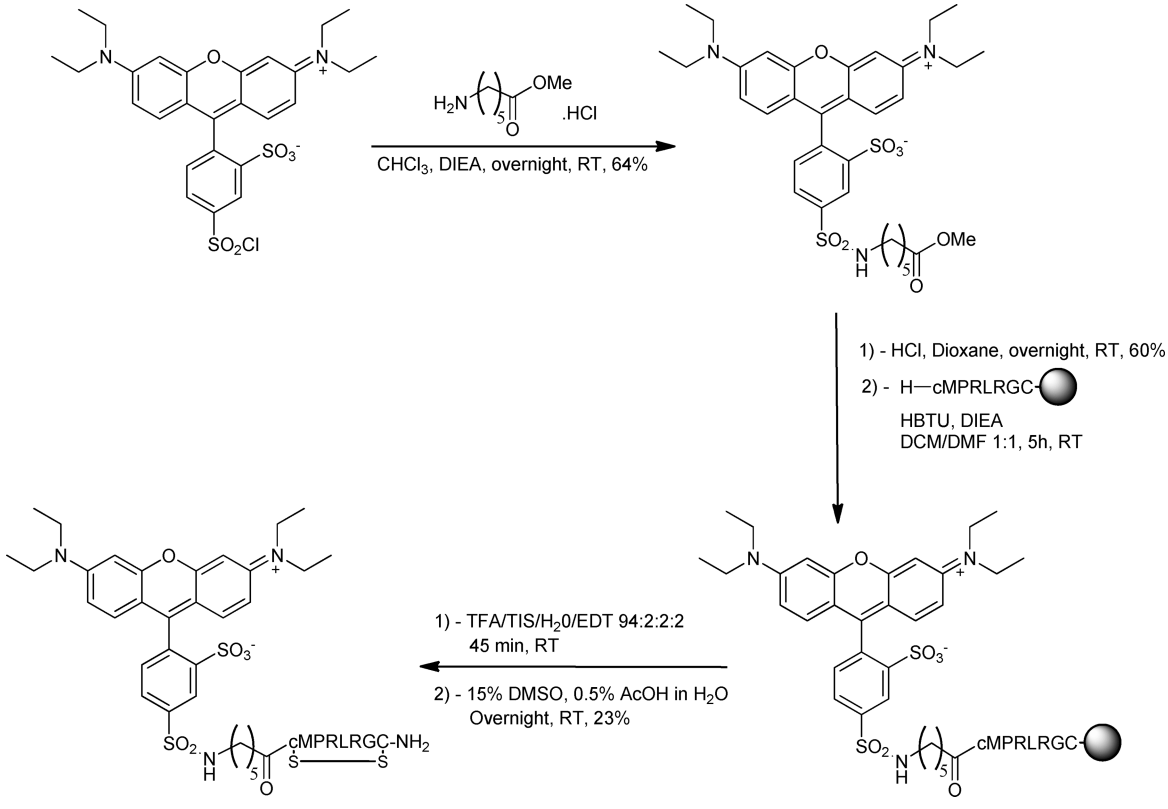

First, methyl aminohexanoate hydrochloride (1.4 equiv) was coupled to commercial Lissamine Rhodamine B sulfonyl chloride in the presence of DIEA (2.2 equiv). The methyl ester was hydrolyzed in 2 M HCl to give the acid form of the Rhodamine Red-X. Rhodamine Red-X (2 equiv) was then coupled directly to the peptides on resin for 5 h using HBTU (2 equiv) and DIEA (2 equiv). Finally, the conjugates were deprotected and removed from the resin and the disulfide bridge was obtained by oxidation using DMSO (Scheme 7).

The resulting fluorescent peptides, being more hydrophobic than Rhodamine Red-X alone, were dissolved in DMSO at 5 mM prior to further dilution for intravenous administration

dx.doi.org/10.1021/jm2014919 | J. Med. Chem. 2012, 55, 2227–2241

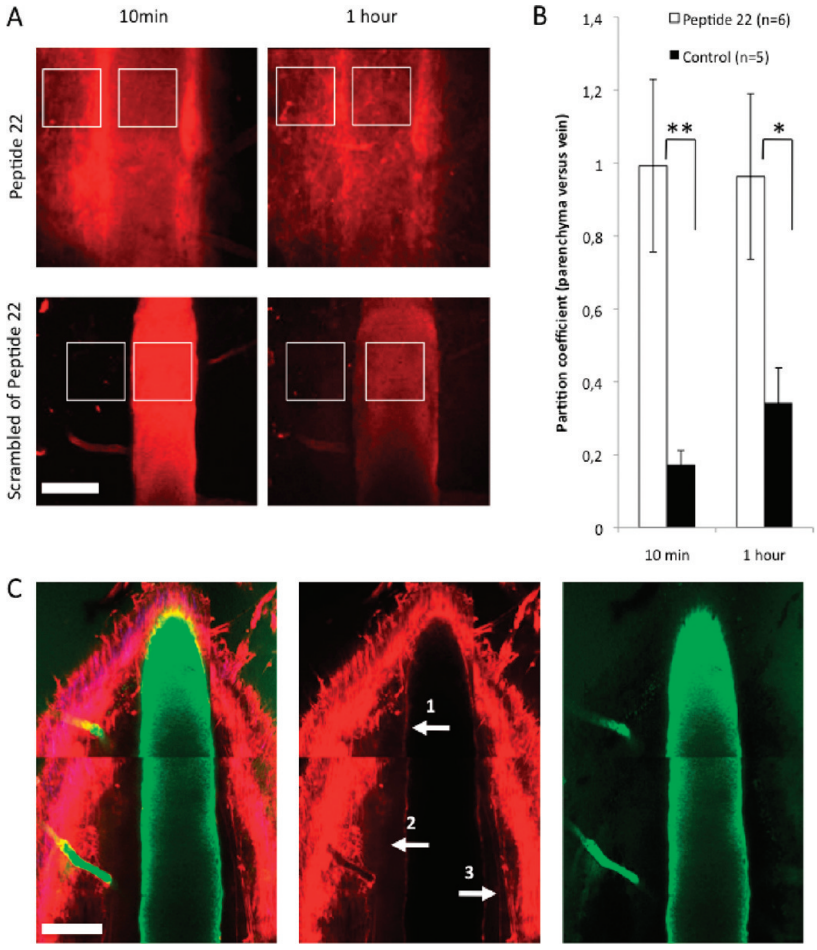

Figure 6. In vivo assay of blood−spinal cord barrier selective permeability to peptide **22**. (A) Two-photon microscopy images of the dorsal spinal cord in living mice after iv injection of fluorescent peptide **22** tagged with Rhodamine Red-X (top) or injection of corresponding fluorescent scrambled peptide (bottom). Images were acquired either 10 min or 1 h after injection. Note the perivascular accumulation of fluorescence in the neuronal parenchyma only in the case of peptide **22**. White boxes represent typical area selected for quantitative analysis of fluorescence distribution. (B) Average values of the ratio between perivascular and intravascular fluorescence for two different time points after injection of either peptide **22** or control solutions. Controls include solutions with fluorescent scrambled peptide or with Rhodamine Red-X molecules alone. (C) Bicolour single plane image acquired 10 min after co-injection of peptide **22** and fluorescein dextran, 70 kDa. Corresponding monochrome images outline peptide **22** accumulation in vessel wall (1), diffuse staining of the parenchyma (2), intense staining of fibrous structures (3), and the absence of such staining in the green channel (right). Scale bars, 100 mm; ∗, $p < 0.05$; ∗∗, $p < 0.02$.

to the animal. Injectable solution was obtained by a 30-fold dilution in phosphate buffer saline (PBS) of this stock DMSO solution. Given an injected volume of 200 μL per animal, the DMSO dose per mouse was 10-fold lower than the reported lethal dose 50 (3100 mg/kg iv mouse data, Sigma-Aldrich, i.e., 100 mg/mouse).

Biodistribution of the fluorescent peptides was then assessed directly in the superficial dorsal spinal cord of anesthetized animals (first 100 μm below surface) either 10 min after systemic injection or at longer time points ranging from 40 to 70 min postinjection. The lumen of blood vessels was homogeneously highlighted by the red fluorescent solution. However, within 10 min after injection, the fluorescence signal clearly accumulated in vessel walls and in extravascular fibrous structures whereas diffuse background fluorescence appeared in the perivascular environment (n = 6, Figure 6A,C).

Whether the stained fibrous structures represent axons or extracellular matrix fibers remains to be clarified. BBB and BSCB disruption were not involved in this process as discussed below.

Indeed, green fluorescence leakage was absent when fluorescein dextran, 70 kDa, was co-injected with peptide **22** (Figure 6C). Moreover, red fluorescence accumulation/leakage was not observed 10 min after injection of either Rhodamine Red-X alone (n = 2) or a rhodamine labeled scrambled peptide of **22** with no affinity for the LDLR in vitro (n = 3). The fast fluorescence redistribution after systemic injection of peptide **22** was neither due to the diffusion of cleaved fluorescence tags nor due to the synergic entraining of Rhodamine Red-X tag bound on the peptide. Instead the fluorescent peptide as a whole crossed the BSCB in a sequence dependent manner, as expected from a receptor dependent process.

Even if both Rhodamine Red-X and the scrambled peptide of **22** exhibited progressive diffusion from vessels to the parenchyma on longer time scales, their diffusion was modest relative to peptide **22** (Figure 6B). One hour after injection the average fluorescence measured in the parenchyma was only one-third (0.34 ± 0.09, n = 5) of the average fluorescence measured in a similar volume of venous blood for Rhodamine Red-X and scrambled peptide of **22**. The ratio was close to unity 10 min after injection of peptide **22** (0.99 ± 0.24, n = 6; Figure 6B),

dx.doi.org/10.1021/jm2014919 | J. Med. Chem. 2012, 55, 2227−2241

indicating that concentration equilibrated fast across the vessel wall. Altogether our in vivo data indicated that peptide **22** has the unique ability to quickly cross the BSCB.

CONCLUSION

Noninvasive delivery of therapeutics to the CNS is currently a major challenge in medicinal chemistry. In this field, RMT is a serious option to improve CNS targeting and delivery of (bio)pharmaceuticals by designing new ligands of endocytic receptors as potential vectors. Chemical optimization of the cyclic peptide **1**, isolated from the screening of a phage display library directed toward the hLDLR, first led to peptide **22** with a highly increased binding affinity for the target receptor and with no binding competition observed for this ligand with the endogenous LDL. Further chemical optimization of peptide **22** led to the synthesis of 60 analogues, including the introduction of non-natural amino acids, disulfide bridge analogues/isosteres, and peptide bond modifications. Binding affinity of these analogues for the hLDLR was evaluated by in vitro displacement of the S-tagged reference peptide **22**. Some of them demonstrated a substantial increase in binding affinity, as exemplified by compound **60**, which displaced 91% of the S-tagged reference peptide **22** at 10 μM. Overall results showed that the spatial conformation of the peptide plays a key role in the binding affinity for the hLDLR. Then NMR-oriented structural studies followed by docking experiments on peptide **22** were carried out to identify four putative binding regions on the extracellular hLDLR domain that provide tracks for further site-directed mutagenesis experiments. Within the framework of discovering new peptide-based vectors for CNS targeting, in vivo crossing of CNS physiological barriers was demonstrated in the spinal cord by biphoton microscopy imaging for peptide **22**. Altogether, these promising results will lead us to investigate the design and the biological evaluation of conjugates with a CNS-therapeutic cargo unable to cross the BBB and the BSCB by itself.

EXPERIMENTAL SECTION

Materials and Methods. Fmoc-amino acids were supplied from Iris Biotech (Marktredwitz, Germany). All other amino acids and reagents were purchased from Sigma-Aldrich (Saint-Quentin Fallavier, France) and Carlo Erba (Peypin, France). Peptide assembly was carried out using the Liberty (CEM) microwave synthesizer by solid phase peptide synthesis (SPPS) in Fmoc/^{t}Bu strategy. Fmoc-Rink amide aminomethylpolystyrene resin cross-linked with 1% DVB (loading, 0.45 mmol·g^{-1}) purchased from Iris Biotech (Marktredwitz, Germany) was used as solid support. Preparative reverse-phase high performance liquid chromatography (RP-HPLC) was carried out on a Waters Prep LC4000 system with Guard-Pak cartridges Delta-Pak C18 (25 mm × 10 mm). The crude products were purified by preparative RP-HPLC using a gradient going from 0% CH_3CN (0.1% TFA) to 15−30% CH_3CN (0.1% TFA) in 5 min, then to 25−70% CH_3CN (0.1% TFA) in 20 min at a flow rate of 20 mL/min. Purified products were then lyophilized in H_2O/CH_3CN (1:1) (0.1% TFA). LC/ESIMS was performed on a Platform II Micromass ZQ preceded by an HPLC Waters Alliance 2690 system. This HPLC system used a C18 Chromolith Flash (4.6 mm × 25 mm) column with a 2.5 min gradient going from 100% H_2O (0.1% HCO_2H) to 100% CH_3CN (0.1% HCO_2H) at a flow rate of 3 mL·min^{-1}. Analytical HPLC was performed on a Waters 1525 HPLC system equipped with a Chromolith SpeedRod RP-18 (4.6 mm × 50 mm) column with a 3 min gradient going from 100% H_2O (0.1% TFA) to 100% CH_3CN (0.1% TFA) at a flow rate of 5 mL·min^{-1}. All compounds reported are of at least 95% purity. ^{1}H, ^{13}C, HSQC ^{1}H/^{13}C, HMBC ^{1}H/^{13}C, COSY ^{1}H/^{1}H, and TOCSY selective 1D and NOESY ^{1}H/^{1}H NMR spectra were recorded on a 600 MHz Bruker Advance III nuclear magnetic resonance (NMR) spectrometer (^{1}H 600 MHz, ^{13}C 75 MHz) in DMSO-d_6. Chemical shifts are reported in parts per million (δ units) downfield/upfield from residual DMSO (δ 2.50 and 39.5). Coupling constants (J) are reported in hertz (Hz). ESI HRMS mass spectra were recorded on a Q-Tof I mass spectrometer (Waters, Manchester, U.K.) fitted with an electrospray ion (ESI) source.

The FRETWorks S-Tag assay kit was obtained from Merck (Darmstadt, Germany). All culture medium, culture additives, and phosphate buffer saline (PBS) were obtained from Invitrogen (Carlsbad, CA, U.S.). CHO-hLDLR-DsRed2 cell line was developed by Vect-Horus (Marseille, France). CHO-hLDLR-DsRed2 cells were maintained in Ham-F12 medium supplemented with 5% fetal bovine serum, 100 U/mL penicillin/streptomycin, and 500 μg/mL Geneticin in 75 cm^2 culture flasks at 37 °C under humidified atmosphere with 5% CO_2.

General Procedure for Peptide Synthesis. Peptides were synthesized on solid phase using a Liberty (CEM) microwave peptide synthesizer on a 0.1 mmol scale. Fmoc-Rink amide aminomethylpolystyrene resin (0.222 g, loading of 0.45 mmol·g^{-1}) was swollen in DCM/DMF (1:1) for half an hour. Initial deprotection of the resin and stepwise assembly were performed in the microwave using standard Fmoc peptide chemistry. Finally, the beads were washed with DCM, MeOH twice, and DCM. Acetylation of the N-terminus of the final peptides on solid support was carried out in an Ac_2O/DCM (1:1) mixture for 5 min twice. The beads were further washed three times with DCM and dried under vacuum. The beads were then treated with TFA/TIS/H_2O/EDT (94:2:2:2) at room temperature for 1 h. The cleavage solution was recovered, concentrated under N_2 flow, and precipitated three times in diethyl ether. The crude products were dissolved in an H_2O/CH_3CN (1:1) (0.1% TFA) mixture and lyophilized. To form the disulfide bridge, peptides were then dissolved in 0.5% aqueous AcOH (concentration of 0.5 mg of peptide per mL) with 3% 2 M $(NH_4)_2CO_3$ and 15% DMSO at room temperature for 24 h. The crude products were purified by preparative RP-HPLC. The final products were characterized by HPLC and LC/ESIMS (Supporting Information). All compounds showed ≥95% purity. Peptide **22** was further characterized by HRMS spectrometry and ^{1}H, ^{13}C, TOCSY, COSY, and NOESY NMR (see Supporting Information). **22** HRMS (ESI) m/z: calcd for $C_{38}H_{67}N_{15}O_9S_3$ $[M + H]^+$ 974.4487, found $[M + H]^+$ = 974.4473.

Synthesis of the Amide Bridge 35. The linear peptide Ac-D-Dap(Alloc)-Met-Pro-Arg-Leu-Arg-Gly-Asp(OAll)-NH_2 (0.1 mmol) was assembled on Rink amide (loading, 0.45 mmol·g^{-1}) using Fmoc peptide chemistry. The resin was swollen in DCM for 10 min. Phenylsilane (2.4 mmol, 296 μL) dissolved in 1 mL of DCM and tetrakis(triphenylphosphine)palladium(0) (29 mg, 0.25 mmol) were added. The mixture was left at room temperature for 30 min and the resin washed with DCM, DMF, and DCM again. The operation was repeated once more. The resin was then suspended in NMP. HBTU (228 mg, 0.6 mmol), HOBt (92 mg, 0.6 mmol), and NMM (1.2 mmol, 132 μL) were successively added, and the mixture was stirred at room temperature for 2 h. The resin was washed with DCM, DMF, DCM, and NMP. The peptide was cleaved from the support using TFA/TIS/H_2O/EDT (94:2:2:2) for 45 min. The cleavage solution was recovered, concentrated under N_2 flow, and precipitated three times in diethyl ether. The crude product was dissolved in H_2O/CH_3CN (1:1) (0.1% TFA) and lyophilized to give a white powder. The crude product was purified by preparative RP-HPLC. The fractions were lyophilized to give a white solid. MS (ESI) m/z: calcd for $C_{39}H_{68}N_{16}O_{10}S$ $[M + H]^+$ 953.50, found $[M + H]^+$ = 953.7 ; $[M + 2H]^{2+}$ = 477.4.

Synthesis of the Lanthionine Bridge 36. The cyclic peptide **22** (34 mg, 3.5 × 10^{-5} mol) was dissolved in 35 mL of TEA/H_2O (9:1). The mixture was stirred at room temperature overnight and lyophilized. The crude product was purified by preparative RP-HPLC and lyophilized in H_2O/CH_3CN (1:1) (0.1% TFA) to give a white powder. MS (ESI) m/z: calcd for $C_{38}H_{67}N_{15}O_9S_2$ $[M + H]^+$ 941.47, found $[M + H]^+$ = 941.7; $[M + 2H]^{2+}$ = 471.9.

Synthesis of the Alkene Bridge 37. The cleaved linear peptide Ac-D-Hag-Met-Pro-Arg-Leu-Arg-Gly-Hag-NH_2 was assembled on Rink amide resin (loading, 0.45 mmol·g^{-1}) using Fmoc peptide chemistry and standard cleaving protocol. The peptide (30 mg, 3.1 × 10^{-5} mol)

dx.doi.org/10.1021/jm2014919 | J. Med. Chem. 2012, 55, 2227−2241

was dissolved in 10 mL of an acetic acid/anhydrous DCM (1:1) mixture in an appropriate microwave vessel. 100 mg of LiCl was added under nitrogen, followed by the second generation Hoveyda−Grubbs catalyst (3 mg, 4.7×10^{-6} mol). The vessel was irradiated under microwave for 1 h at 100 °C with a maximum power of 40 W. Then 10 mL of a solution of H_2O/TFA 0.1% was added. The organic phase was extracted three times with 10 mL of H_2O/TFA, 0.1%. The aqueous phases were gathered and purified by preparative RP-HPLC. After lyophilization, a white powder was obtained. MS (ESI) *m/z*: calcd for $C_{40}H_{69}N_{15}O_9S$ $[M + H]^+$ 936.51, found $[M + H]^+$ = 936.77 ; $[M + 2H]^{2+}$ = 468.91.

Synthesis of the 1,2,3-Triazole Bridge 38. The linear peptide Ac-D-Pra-Met-Pro-Arg-Leu-Arg-Gly-Aha-NH_2 (0.1 mmol) was assembled on Rink amide resin (loading, 0.45 mmol·g^{-1}) using Fmoc peptide chemistry. The supported peptide (1.004 g, 2.61×10^{-4} mol) was swollen in THF for 30 min. Copper iodide (100 mg, 5.22×10^{-4} mol) and DIEA (500 μL, 2.8×10^{-3} mol) were added to the resin. The mixture was stirred at 35 °C for 3 days. The resin was washed with DMF (3 times), H_2O/THF (1:1) (3 times), water saturated with EDTA (3 times), H_2O/THF (1:1) (3 times), CH_3CN (3 times), and DCM (3 times). The peptide was cleaved from the support using a TFA/TIS/H_2O/EDT (94:2:2:2) mixture for 45 min. The cleavage solution was recovered, concentrated under N_2 flow, and precipitated three times in diethyl ether. The crude product was dissolved in H_2O/CH_3CN (1:1) (0.1% TFA) and lyophilized to give a white powder. MS (ESI) *m/z*: calcd for $C_{41}H_{70}N_{18}O_9S$ $[M + H]^+$ 991.53, found $[M + 2H]^{2+}$ = 496.5.

Synthesis of the Guanidinium Bridge 39. *Alloc Deprotection.* The linear peptide Ac-D-dap(Alloc)-Met-Pro-Arg-Leu-Arg-Gly-Dap(Mtt)-NH_2 was assembled on Rink amide (loading, 0.45 mmol·g^{-1}) using Fmoc peptide chemistry. The supported peptide (1.67 g, 2.12×10^{-4} mol) was swollen in anhydrous DCM for 10 min. $Pd[PPh_3]_4$ (49 mg, 4.24×10^{-5} mol) and phenylsilane (552 mg, 5.1×10^{-3} mol) were added away from light. The mixture was stirred for 4 h at room temperature. The resin was washed with DCM, DMF, and DCM twice. The resin was dried under vacuum. The reaction was monitored by cleaving 10 mg of dried resin with TFA/TIS/H_2O/EDT (94:2:2:2).

Synthesis of the Isothiocyanate Derivative. The resin from the previous reaction was swollen in DCM for 10 min. DPT (di-2-pyridyl thionocarbonate) (246 mg, 1.06×10^{-3} mol) was added. The mixture was stirred for 12 h at room temperature. The resin was washed with DMF (three times) and DCM (three times). The reaction was monitored by cleaving 10 mg of dried resin with TFA/TIS/H_2O/EDT (94:2:2:2).

Synthesis of the Thiourea Bridge. The Mtt protective group was removed using DCM/TFE/AcOH (7:2:1) over six rounds of 20 min at room temperature and renewing the mixture after each round. The resin was washed with DMF (three times), DCM (three times), and MeOH (three times). It was then swollen in THF for 10 min. Triethylamine (98 mg, 8.48×10^{-4} mol) was added, and the mixture was refluxed for 3 h. It was then stirred for 12 h at room temperature. The resin was washed with DMF (three times), DCM (three times) and dried under vacuum. The reaction was monitored by cleaving 10 mg of dried resin with TFA/TIS/H_2O/EDT (94:2:2:2).

Synthesis of the S-Methyl Thiourea Bridge. The supported thiourea (918.53 mg, 1.42×10^{-4} mol) was swollen in DMF for 10 min. Then 6 mL of a 0.2 M methyl iodide solution in DMF was added, and the mixture was stirred for 1 h at room temperature. The operation was repeated twice. The resin was washed with DMF (three times) and DCM. The reaction was monitored by cleaving 10 mg of dried resin with TFA/TIS/H_2O/EDT (94:2:2:2).

Synthesis of the Guanidinium Bridge. The supported resin from the previous reaction was swollen in anhydrous DMSO. The DMSO was filtered, and 2 M $(NH_4)_2CO_3$ in anhydrous DMSO solution was added to the resin. The mixture was stirred at 80 °C for 12 h. The resin was washed with DCM (three times), DMF (three times), DCM (twice) and dried under vacuum. The peptide was cleaved from the support using TFA/TIS/H_2O/EDT (94:2:2:2) for 45 min. The cleavage solution was recovered, concentrated under N_2 flow, and precipitated three times in diethyl ether. The crude product was dissolved in an H_2O/CH_3CN (1:1) (0.1% TFA) mixture and lyophilized to give a white powder. The crude product was purified by preparative RP-HPLC. The fractions were lyophilized to give a white solid. MS (ESI) *m/z*: calcd for $C_{39}H_{70}N_{18}O_9S$ $[M + H]^+$ 966.53, found $[M + 2H]^{2+}$ = 484.4; $[M + 3H]^{3+}$ = 323.4.

General Procedure for the Synthesis of Pseudo-Peptides 79−83. The appropriate Fmoc amino acids (1×10^{-3} mol), protected on their side chains when needed, were dissolved in 30 mL of DCM. The Weinreb amide (293 mg, 3×10^{-3} mol), DIEA (517 mg, 4×10^{-3} mol), and then BOP (1.328 g, 3×10^{-3} mol) were added successively. The mixture was stirred for 3 h at room temperature. The solvent was evaporated under vacuum, and the crude product was dissolved in water and ethyl acetate. The organic layer was washed with 1 M $KHSO_4$ (three times), saturated $NaHCO_3$, and brine. The organic layer was then dried over anhydrous Na_2SO_4 and evaporated under vacuum. The Weinreb amide was obtained as a colorless solid. Without further purification, this latter derivative (0.4×10^{-3} mol) and lithium aluminum hydride (77 mg, 2.4×10^{-3} mol) were dissolved in 20 mL of anhydrous THF at 0 °C. The mixture was stirred at 0 °C for 15 min. It was then quenched with 25 mL of 1 M $KHSO_4$ added dropwise. The aqueous layer was extracted three times with 20 mL of diethyl ether. The organic layers were gathered, dried over anhydrous Na_2SO_4, and evaporated under vacuum. A colorless oil was obtained. The aldehyde was used straight away in the next step without further purification. The precursor peptide (0.1 mmol) was assembled on Rink amide resin (loading, 0.45 mmol·g^{-1}) using standard Fmoc peptide chemistry. This resin was swollen in anhydrous DMF with 1% acetic acid. The aldehyde (0.4×10^{-3} mol) and sodium cyanoborohydride (50 mg, 0.8×10^{-3} mol) were added under nitrogen. The mixture was stirred at room temperature overnight. The resin was washed with DMF (twice), DCM (twice), MeOH (twice), and DCM (twice) and dried under vacuum. The reaction was monitored by cleaving 10 mg of dried resin with TFA/TIS/H_2O/EDT (94:2:2:2). The remaining residues were added to the peptidic chain using standard microwave SPPS. The final peptide was cleaved from the resin following the general procedure for peptide synthesis. To form the disulfide bridge, peptides were then dissolved in 0.5% aqueous AcOH (concentration of 0.5 mg of peptide per mL), with 3% 2 M $(NH_4)_2CO_3$ and 15% DMSO at room temperature for 24 h. The crude products were purified by preparative RP-HPLC. **79**, MS (ESI) *m/z*: calcd for $C_{38}H_{69}N_{15}O_8S_3$ $[M + H]^+$ 960.48, found $[M + H]^+$ = 960.5; $[M + 2H]^{2+}$ = 480.9; $[M + 3H]^{3+}$ = 321.0. **80**, MS (ESI) *m/z*: calcd for $C_{38}H_{69}N_{15}O_8S_3$ $[M + H]^+$ 960.48, found $[M + H]^+$ = 960.3; $[M + 2H]^{2+}$ = 480.8; $[M + 3H]^{3+}$ = 320.95. **81**, MS (ESI) *m/z*: calcd for $C_{38}H_{69}N_{15}O_8S_3$ $[M + H]^+$ 960.48, found $[M + H]^+$ = 960.5; $[M + 2H]^{2+}$ = 480.9; $[M + 3H]^{3+}$ = 321.0. **82**, MS (ESI) *m/z*: calcd for $C_{38}H_{69}N_{15}O_8S_3$ $[M + H]^+$ 960.48, found $[M + H]^+$ = 960.41; $[M + 2H]^{2+}$ = 480.87; $[M + 3H]^{3+}$ = 320.95. **83**, MS (ESI) *m/z*: calcd for $C_{38}H_{69}N_{15}O_8S_3$ $[M + H]^+$ 960.48, found $[M + H]^+$ = 960.41; $[M + 2H]^{2+}$ = 480.87; $[M + 3H]^{3+}$ = 320.95.

In Vitro Binding Assay. The FRETWorks S-Tag assay (Merck, Darmstadt, Germany) was based on the interaction of the S-tagged peptides with an enzymatically inactive ribonuclease S protein. This resulted in the reconstitution of a fully functional ribonuclease S-enzyme, which cleaved a short chimeric ribonucleotide/deoxyribonucleotide having a fluorophore on the 5′ end and a quencher on the 3′ end. Cleavage of this substrate by the reconstituted ribonuclease decoupled the quencher from the fluorophore, which became fluorescent (excitation 492 nm, emission 520−535 nm) and could be quantified in a Beckton Dickinson DU800 spectrophotometer. For the assay, peptides (10 μM) were incubated with the CHO-hLDLR-RFP cells (800 000 cells per well of a six-well plate) in triplicate in Ham-F12, 1% bovine serum albumin (BSA) for 1 h at 37 °C, 5% CO_2.

Several internal controls solutions were prepared:

(i) HamF12−1% BSA medium + S-tagged scramble peptide (evaluation of nonspecific binding of any peptide comprising the S-Tag)

(ii) HamF12−1% BSA medium + S-tagged reference peptide **1** or **22** (evaluation of nonspecific + specific binding, where the

100% binding is obtained after subtraction of the nonspecific, background signal)

(iii) HamF12−1% BSA medium + S-tagged reference peptide **1** or **22** + scramble peptide (evaluation of nonspecific competition between the peptide of interest and a control peptide)

(iv) HamF12−1% BSA medium + S-tagged reference peptide **1** or **22** + untagged reference peptide (evaluation of specific binding displacement, where the 50% binding is obtained after subtraction of the nonspecific background signal)

The cells were washed with PBS in order to eliminate any trace of nonfixed peptide, scrapped, centrifuged (5 min at 300*g*), and lysed in 80 μL of PBS 0.1% Triton X100 (Sigma). An amount of 20 μL of cell extracts was mixed with 180 μL of reaction mix (1× FRET assay buffer, FRET ArUAA substrate, and S-Tag grade S-protein). This FRET assay was used to test the potential for neosynthesized peptides (10 μM) to displace during 1 h at 37 °C the S-tagged peptide **1** (10 μM) bound to the cells and then to displace the new reference S-tagged peptide **22**. Calculated values were the mean of at least three points. A maximum deviation of 10% of control compared to its theoretical value was tolerated.

Plasma Stability. The in vitro plasma stability of peptides **19**, **22**, **57**, **61**, **62**, **76**, and **78** was determined by spiking freshly collected Swiss mouse blood with each compound (n = 3), resuspended beforehand in 0.9% NaCl, at the nominal concentration of 2 μM. For each peptide, an analytical method was developed for detection and quantification in mouse plasma using LC−MS/MS. Aliquots containing an adequate volume of the compound/plasma mixture were placed separately into extraction tubes and incubated at 37 °C for 0, 0.5, 1, 2, 5, and 8 h. At the appropriate time points, a volume of 250 μL of blood was withdrawn and centrifuged (5 min, 2500 rpm, 10 °C). A volume of 100 μL of the supernatant was collected, and 10 μL of formic acid and 300 μL of acetonitrile were added for acidification and protein precipitation, respectively. After centrifugation, the supernatant was analyzed using a Shimadzu LC equipment coupled to an API 4000 triple quadrupole mass spectrometer (Applied Biosystems). For separation an amount of 25 μL of the extracted samples was injected into the HPLC system (Chromolith C18, 100 mm × 3 mm; 1 mL/min; gradient, mobile phase A of 0.1% formic acid in water, mobile phase B of 0.05% trifluoroacetic acid in acetonitrile). Tandem mass spectrometry was performed using an electrospray ionization (ESI) interface operating in the positive ionization mode. Individual mass transitions (m/z ratios) were selected based on both highest sensitivity and lowest background noise. Calibration curves were performed twice, namely, before and after processing of test samples to ensure repeatability of the analytical procedure with a lower limit of quantification (LLOQ) set at 25−50 nM. As the degradation kinetics of all compounds tested were best described by an exponential regression curve (i.e., first-order reaction kinetics), in vitro half-lives ($t_{1/2}$) were estimated on the basis of the following equation: $C(t) = C_0e^{-kt}$, with $t_{1/2} = \ln 2/k$.

NMR Spectroscopy. NMR samples were prepared by dissolving 4.53 mg of the peptide **22** in DMSO-d_6 (100 μL). ^{1}H, ^{13}C, DQF-COSY, selective 1D TOCSY, HSQC, HMBC, and NOESY spectra were recorded at 300 K on a 600 MHz Advance III Bruker instrument (see Supporting Information). Mixing times of 300 ms for selective 1D TOCSY and 700 ms for NOESY were applied. The DQF-COSY spectrum was acquired with 2048 data points in the direct dimension and 512 increments with 16 scans. The HSQC spectrum was acquired with 2048 data points in the direct dimension and 512 increments with 16 scans. The HMBC spectrum was acquired with 4096 data points in the direct dimension and 512 increments with 32 scans. The NOESY spectrum was acquired with 4096 data points in the direct dimension and 1024 increments with 64 scans. Spectral processing was carried out using the software TopSpin, version 2.1.

Modeling of Peptide 22. Molecular models of the cyclo-Cys-Met-Pro-Arg-Leu-Arg-Gly-Cys were built with the CHARMM software and force field.[58] Proton−proton interatomic distances were derived from the NMR experiments and injected as NOE constraints in the models. The used constraints were depicted in Figure 3. Because of the high energy barriers inherent to cyclopeptides, we used an energy minimization protocol that we described elsewhere[59] instead of classical high temperature molecular dynamics or simulated annealing protocols. The method consists of testing almost all the possible orientations of the main chain by forcing each residue to be in one of the 10 most-frequented φ:ψ regions of the Ramachandran plot, through the use of harmonic constraints of 5000 kcal·mol^{-2}·Å^{-2}. All the possible combinations were tested. The cysteines involved in the disulfide bridge as well as the Gly residue were kept free to move. For the proline residue, only two regions were explored whereas the ensemble of the 10 possible regions was tested for other residues. For this peptide, the protocol led to 10 × 2 × 10 × 10 × 10 = 20 000 different conformations. This adiabatic map method is thought to be more efficient in identifying all the possible energy minima on the energy surface of such a short peptide. Minimizations were performed by combining steepest descent (5000 steps) and adopted based Newton−Raphson (5000 steps) algorithms until an energy gradient of 1 kcal·mol^{-1} was reached. The GBSW parameters were used in all steps of the minimization process to properly mimic the presence of the surrounding water. Harmonic constraints of the same order as those used for φ:ψ dihedrals (5000 kcal·mol^{-2}·Å^{-2}) were added to maintain all the peptide amide bonds in the trans conformation through the process of conformational sampling. Of course, because many of the φ:ψ combinations are not possible and lead to energetically unrealistic models, the energy of each produced model was reminimized in a second step, after having removed all the φ:ψ constraints but still retaining NOE and peptide bonds constraints. The internal energy of each obtained model was conserved for further analysis. Molecular models were graphed and structurally fit with VMD[60] or Pymol (http://www.pymol.org/) software. Only conformers that were fully respecting the whole set of NOE constraints were retained. Clustering of this defined set of conformations was performed with PTRAJ, as implemented in AmberTools.[61]

Docking. Docking of the three representative conformers of the peptide was first performed using the Vina software[62] and using the X-ray structure PDB 3M0C as a target.[63] This structure available in the Protein Data Bank describes parts of the extracellular domain of the LDL receptor. For a better exploration of the conformational space, two different docking regions were first defined. The first one encompassed the atoms of the β-barrel plus those of the EGF domain C in a sphere of 35 Å around Ile501 (green surface in Figure 4). The second one corresponded to the EGF domains A and B in a sphere of equal radius but this time centered on Cys317 (orange surface in Figure 4). The aim of this first blind docking protocol was to identify the putative regions of binding on the whole surface of the receptor. It was verified that the method successfully converged, by repeating the calculations three times. In a second step, the Autodock software was used to refine the docking of the peptide in each of the so-identified regions. On each of these regions, 50 docking runs were performed for each of the three peptide conformers using the Lamarckian genetic algorithm and a standard grid precision of 0.375 Å.

In Vivo Biphoton Microscopy Assay. Our experimental procedures are approved by the Ethics Committee of the Medical Faculty of Marseille and conform to National and European regulations (EU Directive No. 86/609). All efforts were made to minimize animal suffering and reduce the number of animals used.

Adult C57-Bl6 mice (>7 weeks) were prepared according to the protocol detailed earlier.[64] Briefly, once deeply anesthetized with a mixture of ketamine-xylasine (100 mg/kg, 10 mg/kg), freely breathing mice were placed in a modified Cunningham spinal cord holder and subjected to a thoracic T13 laminectomia. Then 200 μL of peptide solution (167 μM in DMSO + PBS) was injected intravenously before placing the animal under a Zeiss Apochromat 20× (NA = 1.0) water immersion objective. An additional 50 μL of fluorescein dextran solution (70 kDa, 280 μM in PBS) was occasionally co-injected with the peptide solution. A Zeiss LSM 7MP microscope coupled to a femtosecond pulsed infrared laser (Mai-Tai, Spectra-Physics, Santa Clara, CA) tuned at 840 nm was used in these experiments. Emission was collected between 500−550 nm and 575−640 nm. Image acquisition was started 10 min after iv injection and was repeated until 70 min after initial injection. Animals were overdosed with anesthetic at the end of the imaging session.

Stacks of 8-bit images at 5 μm intervals on the *Z*-axis were acquired over a depth of 200 μm. Volumes used for analysis were manually registered and trimmed to compensate for suboptimal repositioning. The resulting volumes were then sum-projected over 100 μm using ImageJ software. For each animal, the average fluorescence was evaluated in pairs of 100 μm^3 volumes chosen respectively in the central dorsal vein or in the closest extravascular parenchyma. Measures from three different pairs of volumes were averaged for each mouse. Statistical significance was tested using Mann–Whitney *U*-test.

■ ASSOCIATED CONTENT

Supporting Information

Experimental details of the peptide synthesis by microwave irradiation, structure of non-natural amino acids, analytical data of all synthesized compounds, and spectral data of compound **22**. This material is available free of charge via the Internet at http://pubs.acs.org.

■ AUTHOR INFORMATION

Corresponding Author

*Phone: +33(0)411759599. Fax: +33(0)467548654. E-mail: vincent.lisowski@univ-montp1.fr.

Notes

The authors declare no competing financial interest.

■ ACKNOWLEDGMENTS

Financial support for this work was provided in part by the Direction Générale de la Compétitivité, de l'Industrie et des Services (DGCIS) and the Pôle de Compétitivité Eurobiomed (MEDUL project) and the French National Agency for Research (ANR JCC PathoVisu3dyn to F.D.) and the region Languedoc-Roussillon (chercheur d'avenir 2011 grant to V.L.). Vect-Horus' projects are supported in part by grants from the DGCIS, under Grant No. 08 2 90 6182 (MEDUL project), and from the French National Research Agency (ANR), under Grants ANR-09-BIOT-015-01 and ANR-08-MNPS-042-04 (VECtoBrain and TIMPAD projects, respectively). The NICN laboratory is supported by the CNRS and Aix-Marseille Univ and by ANR, under Grants ANR-09-BIOT-015-04 and ANR-08-MNPS-042-01 (VECtoBrain and TIMPAD projects, respectively). We thank Dr. Aurélien Lebrun for the NMR experiments.

■ REFERENCES

(1) Pardridge, W. M. Blood–brain barrier delivery. *Drug Discovery Today* **2007**, *12*, 54–61.

(2) Pardridge, W. M. Why is the global CNS pharmaceutical market so under-penetrated? *Drug Discovery Today* **2002**, *7*, 5–7.

(3) Pardridge, W. M. Blood–brain barrier drug targeting: the future of brain drug development. *Mol. Interventions* **2003**, *3*, 90–105.

(4) Nag, S. Morphology and Molecular Properties of Cellular Components of Normal Cerebral Vessels. In *Blood–Brain Barrier*; Humana Press: NJ, 2003; Vol. *89*, pp 3–36.

(5) de Boer, A. G.; Gaillard, P. J. Strategies to improve drug delivery across the blood–brain barrier. *Clin. Pharmacokinet.* **2007**, *46*, 553–576.

(6) Grammas, P.; Martinez, J.; Miller, B. Cerebral microvascular endothelium and the pathogenesis of neurodegenerative diseases. *Expert Rev. Mol. Med.* **2011**, *13*, e19.

(7) Lipinski, C. A.; Lombardo, F.; Dominy, B. W.; Feeney, P. J. Experimental and computational approaches to estimate solubility and permeability in drug discovery and development settings. *Adv. Drug Delivery Rev.* **2001**, *46*, 3–26.

(8) Hitchcock, S. A.; Pennington, L. D. Structure–brain exposure relationships. *J. Med. Chem.* **2006**, *49*, 7559–7583.

(9) Pardridge, W. M. Drug targeting to the brain. *Pharm. Res.* **2007**, *24*, 1733–1744.

(10) Vlieghe, P.; Lisowski, V.; Martinez, J.; Khrestchatisky, M. Synthetic therapeutic peptides: science and market. *Drug Discovery Today* **2010**, *15*, 40–56.

(11) Pardridge, W. M. The blood–brain barrier: bottleneck in brain drug development. *NeuroRx* **2005**, *2*, 3–14.

(12) Pammolli, F.; Magazzini, L.; Riccaboni, M. The productivity crisis in pharmaceutical R&D. *Nat. Rev. Drug Discovery* **2011**, *10*, 428–438.

(13) Paul, S. M.; Mytelka, D. S.; Dunwiddie, C. T.; Persinger, C. C.; Munos, B. H.; Lindborg, S. R.; Schacht, A. L. How to improve R&D productivity: the pharmaceutical industry's grand challenge. *Nat. Rev. Drug Discovery* **2010**, *9*, 203–214.

(14) Patel, M. M.; Goyal, B. R.; Bhadada, S. V.; Bhatt, J. S.; Amin, A. F. Getting into the brain: approaches to enhance brain drug delivery. *CNS Drugs* **2009**, *23*, 35–58.

(15) De Boer, A. G.; Van der Sandt, I. C.; Gaillard, P. J. The role of drug transporters at the blood–brain barrier. *Annu. Rev. Pharmacol. Toxicol.* **2003**, *43*, 629–656.

(16) Jones, A. R.; Shusta, E. V. Blood–brain barrier transport of therapeutics via receptor-mediation. *Pharm. Res.* **2007**, *24*, 1759–1771.

(17) Visser, C. C.; Stevanović, S.; Voorwinden, L. H.; van Bloois, L.; Gaillard, P. J.; Danhof, M.; Crommelin, D. J. A.; de Boer, A. G. Targeting liposomes with protein drugs to the blood–brain barrier in vitro. *Eur. J. Pharm. Sci.* **2005**, *25*, 299–305.

(18) Wu, D.; Yang, J.; Pardridge, W. M. Drug targeting of a peptide radiopharmaceutical through the primate blood–brain barrier in vivo with a monoclonal antibody to the human insulin receptor. *J. Clin. Invest.* **1997**, *100*, 1804–1812.

(19) Ulbrich, K.; Hekmatara, T.; Herbert, E.; Kreuter, J. Transferrin- and transferrin-receptor-antibody-modified nanoparticles enable drug delivery across the blood–brain barrier (BBB). *Eur. J. Pharm. Biopharm.* **2009**, *71*, 251–256.

(20) Olivier, J.-C. Drug transport to brain with targeted nanoparticles. *NeuroRx* **2005**, *2*, 108–119.

(21) Demeule, M.; Régina, A.; Ché, C.; Poirier, J.; Nguyen, T.; Gabathuler, R.; Castaigne, J.-P.; Béliveau, R. Identification and design of peptides as a new drug delivery system for the brain. *J. Pharmacol. Exp. Ther.* **2008**, *324*, 1064–1072.

(22) Demeule, M.; Currie, J.-C.; Bertrand, Y.; Ché, C.; Nguyen, T.; Régina, A.; Gabathuler, R.; Castaigne, J.-P.; Béliveau, R. Involvement of the low-density lipoprotein receptor-related protein in the transcytosis of the brain delivery vector angiopep-2. *J. Neurochem.* **2008**, *106*, 1534–1544.

(23) Gent, J.; Braakman, I. Low-density lipoprotein receptor structure and folding. *Cell. Mol. Life Sci.* **2004**, *61*, 2461–2470.

(24) Chung, N. S.; Wasan, K. M. Potential role of the low-density lipoprotein receptor family as mediators of cellular drug uptake. *Adv. Drug Delivery Rev.* **2004**, *56*, 1315–1334.

(25) Herz, J. The LDL receptor gene family: (un)expected signal transducers in the brain. *Neuron* **2001**, *29*, 571–581.

(26) Brown, M. S.; Goldstein, J. L. Receptor-mediated endocytosis: insights from the lipoprotein receptor system. *Proc. Natl. Acad. Sci. U.S.A.* **1979**, *76*, 3330–3337.

(27) Dehouck, B.; Fenart, L.; Dehouck, M. P.; Pierce, A.; Torpier, G.; Cecchelli, R. A new function for the LDL receptor: transcytosis of LDL across the blood–brain barrier. *J. Cell Biol.* **1997**, *138*, 877–889.

(28) Ché, C.; Yang, G.; Thiot, C.; Lacoste, M.-C.; Currie, J.-C.; Demeule, M.; Régina, A.; Béliveau, R.; Castaigne, J.-P. New angiopep-modified doxorubicin (ANG1007) and etoposide (ANG1009) chemotherapeutics with increased brain penetration. *J. Med. Chem.* **2010**, *53*, 2814–2824.

(29) Khrestchatisky, M.; David, M.; Molino, Y.; Vlieghe, P. Peptides Derivatives and Use Therefore as Carriers for Molecules in the Form of Conjugates. WO2010046588A1, 2010.

(30) Results from Ala-scan of peptide **19** (% of displaced S-Tag peptide **1**): Ac-AMPRLRGC-NH_2 (0%), Ac-[CAPRLRGC]$_c$-NH_2 (7%), Ac-[CMARLRGC]$_c$-NH_2 (0%), Ac-[CMPALRGC]$_c$-NH_2

(0%), Ac-[CMPRARGC]$_c$-NH_2 (28%), Ac-[CMPRLAGC]$_c$-NH_2 (0%), Ac-[CMPRLRAC]$_c$-NH_2 (34%), Ac-CMPRLRGA-NH_2 (0%),
(31) Armishaw, C. J.; Daly, N. L.; Nevin, S. T.; Adams, D. J.; Craik, D. J.; Alewood, P. F. Alpha-selenoconotoxins, a new class of potent α7 neuronal nicotinic receptor antagonists. *J. Biol. Chem.* **2006**, *281*, 14136−14143.
(32) Cerovsky, V.; Wunsch, E.; Brass, J. Enzymatic semisynthesis of dicarba analogs of calcitonin. *Eur. J. Biochem.* **1997**, *247*, 231−237.
(33) Hase, S.; Morikawa, T.; Sakakibara, S. Synthesis of a biologically active analog of deamino-8-arginine-vasopressin which does not contain a disulphide bond. *Experientia* **1969**, *25*, 1239−1240.
(34) Kambayashi, Y.; Nakajima, S.; Ueda, M.; Inouye, K. A dicarba analog of beta-atrial natriuretic peptide (beta-ANP) inhibits guanosine 3′,5′-cyclic monophosphate production induced by alpha-ANP in cultured rat vascular smooth muscle cells. *FEBS Lett.* **1989**, *248*, 28−34.
(35) Stymiest, J. L.; Mitchell, B. F.; Wong, S.; Vederas, J. C. Synthesis of biologically active dicarba analogues of the peptide hormone oxytocin using ring-closing metathesis. *Org. Lett.* **2003**, *5*, 47−49.
(36) Nestor, J. J. Jr. The medicinal chemistry of peptides. *Curr. Med. Chem.* **2009**, *16*, 4399−4418.
(37) Galande, A. K.; Trent, J. O.; Spatola, A. F. Understanding base-assisted desulfurization using a variety of disulfide-bridged peptides. *Pept. Sci.* **2003**, *71*, 534−551.
(38) Robinson, A. J.; Elaridi, J.; Van Lierop, B. J.; Mujcinovic, S.; Jackson, W. R. Microwave-assisted RCM for the synthesis of carbocyclic peptides. *J. Pept. Sci.* **2007**, *13*, 280−285.
(39) Jacobsen, O.; Klaveness, J.; Petter Ottersen, O.; Amiry-Moghaddam, M. R.; Rongved, P. Synthesis of cyclic peptide analogues of the 3(10) helical Pro138-Gly144 segment of human aquaporin-4 by olefin metathesis. *Org. Biomol. Chem.* **2009**, *7*, 1599−1611.
(40) Hossain, M. A.; Rosengren, K. J.; Zhang, S.; Bathgate, R. A.; Tregear, G. W.; van Lierop, B. J.; Robinson, A. J.; Wade, J. D. Solid phase synthesis and structural analysis of novel A-chain dicarba analogs of human relaxin-3 (INSL7) that exhibit full biological activity. *Org. Biomol. Chem.* **2009**, *7*, 1547−1553.
(41) Illesinghe, J.; Guo, C. X.; Garland, R.; Ahmed, A.; van Lierop, B.; Elaridi, J.; Jackson, W. R.; Robinson, A. J. Metathesis assisted synthesis of cyclic peptides. *Chem. Commun.* **2009**, *3*, 295−297.
(42) Alexandra Le Chevalier, I.; Anna Maria, P.; Michael, C.; Paolo, R. Side chain-to-side chain cyclization by click reaction. *J. Pept. Sci.* **2009**, *15*, 451−454.
(43) Jagasia, R.; Holub, J. M.; Bollinger, M.; Kirshenbaum, K.; Finn, M. G. Peptide cyclization and cyclodimerization by CuI-mediated azide-alkyne cycloaddition. *J. Org. Chem.* **2009**, *74*, 2964−2974.
(44) Himo, F.; Lovell, T.; Hilgraf, R.; Rostovtsev, V. V.; Noodleman, L.; Sharpless, K. B.; Fokin, V. V. Copper(I)-catalyzed synthesis of azoles. DFT study predicts unprecedented reactivity and intermediates. *J. Am. Chem. Soc.* **2004**, *127*, 210−216.
(45) Tornøe, C. W.; Christensen, C.; Meldal, M. Peptidotriazoles on solid phase: [1,2,3]-triazoles by regiospecific copper(I)-catalyzed 1, 3-dipolar cycloadditions of terminal alkynes to azides. *J. Org. Chem.* **2002**, *67*, 3057−3064.
(46) Touati-Jallabe, Y.; Chiche, L.; Hamze, A.; Aumelas, A.; Lisowski, V.; Berthomieu, D.; Martinez, J.; Hernandez, J. F. Cyclic peptides with a diversely substituted guanidine bridge: solid-phase synthesis and structural analysis. *Chem.—Eur. J.* **2011**, *17*, 2566−2570.
(47) Breznik, M.; Grdadolnik, S. G.; Giester, G.; Leban, I.; Kikelj, D. Influence of chirality of the preceding acyl moiety on the cis/trans ratio of the proline peptide bond. *J. Org. Chem.* **2001**, *66*, 7044−7050.
(48) Arg_4 and Arg_6 were sequentially substituted by lysine in the preliminary study based on peptide, and these modifications resulted in a total loss of affinity for the receptor.
(49) Jacobson, K. A.; Marr-Leisy, D.; Rosenkranz, R. P.; Verlander, M. S.; Melmon, K. L.; Goodman, M. Conjugates of catecholamines. 1. *N*-Alkyl-functionalized carboxylic acid congeners and amides related to isoproterenol. *J. Med. Chem.* **1983**, *26*, 492−499.
(50) Martinez, J.; Bali, J. P.; Rodriguez, M.; Castro, B.; Magous, R.; Laur, J.; Lignon, M. F. Synthesis and biological activities of some pseudo-peptide analogues of tetragastrin: the importance of the peptide backbone. *J. Med. Chem.* **1985**, *28*, 1874−1879.
(51) Doulut, S.; Rodriguez, M.; Lugrin, D.; Vecchini, F.; Kitabgi, P.; Aumelas, A.; Martinez, J. Reduced peptide bond pseudopeptide analogues of neurotensin. *Pept. Res.* **1992**, *5*, 30−38.
(52) Lugrin, D.; Vecchini, F.; Doulut, S.; Rodriguez, M.; Martinez, J.; Kitabgi, P. Reduced peptide bond pseudopeptide analogues of neurotensin: binding and biological activities, and in vitro metabolic stability. *Eur. J. Pharmacol.* **1991**, *205*, 191−198.
(53) Ma, S.; Spatola, A. F. Conformations of psi [CH_2NH] pseudopeptides. Cyclo[Gly-Pro psi [CH_2NH]Gly-D-Phe-Pro]-TFA and cyclo[Gly-Pro psi [CH_2NH]Gly-D-Phe-Pro]. *Int. J. Pept. Protein Res.* **1993**, *41*, 204−206.
(54) Fehrentz, J. A.; Heitz, A.; Castro, B. Synthesis of aldehydic peptides inhibiting renin. *Int. J. Pept. Protein Res.* **1985**, *26*, 236−241.
(55) Ganneau, C.; Moulin, A.; Demange, L.; Martinez, J.; Fehrentz, J. A. The epimerization of peptide aldehydes: a systematic study. *J. Pept. Sci.* **2006**, *12*, 497−501.
(56) The binding affinity of peptide **22** for the hLDLR was assessed by Scatchard analysis based on the FRET assay and was estimated at 1.4 μM.
(57) Lefevre, C.; Kang, H. C.; Haugland, R. P.; Malekzadeh, N.; Arttamangkul, S.; Haugland, R. P. Texas Res-X and Rhodamine Red-X, new derivatives of sulforhodamine 101 and Lissamine Rhodamine B with improved labeling and fluorescence properties. *Bioconjugate Chem.* **1996**, *7*, 482−489.
(58) Brooks, B. R.; Brooks, C. L.; Mackerell, A. D.; Nilsson, L.; Petrella, R. J.; Roux, B.; Won, Y.; Archontis, G.; Bartels, C.; Boresch, S.; Caflisch, A.; Caves, L.; Cui, Q.; Dinner, A. R.; Feig, M.; Fischer, S.; Gao, J.; Hodoscek, M.; Im, W.; Kuczera, K.; Lazaridis, T.; Ma, J.; Ovchinnikov, V.; Paci, E.; Pastor, R. W.; Post, C. B.; Pu, J. Z.; Schaefer, M.; Tidor, B.; Venable, R. M.; Woodcock, H. L.; Wu, X.; Yang, W.; York, D. M.; Karplus, M. CHARMM: the biomolecular simulation program. *J. Comput. Chem.* **2009**, *30*, 1545−1614.
(59) Floquet, N.; Héry-Huynh, S.; Dauchez, M.; Derreumaux, P.; Tamburro, A. M.; Alix, A. J. P. Structural characterization of VGVAPG, an elastin-derived peptide. *Biopolymers* **2004**, *76*, 266−280.
(60) Humphrey, W.; Dalke, A.; Schulten, K. VMD: visual molecular dynamics. *J. Mol. Graphics* **1996**, *14* (33−38), 27−28.
(61) Case, D. A.; Cheatham, T. E.; Darden, T.; Gohlke, H.; Luo, R.; Merz, K. M.; Onufriev, A.; Simmerling, C.; Wang, B.; Woods, R. J. The Amber biomolecular simulation programs. *J. Comput. Chem.* **2005**, *26*, 1668−1688.
(62) Trott, O.; Olson, A. J. AutoDock Vina: improving the speed and accuracy of docking with a new scoring function, efficient optimization, and multithreading. *J. Comput. Chem.* **2010**, *31*, 455−461.
(63) Kwon, H. J.; Lagace, T. A.; McNutt, M. C.; Horton, J. D.; Deisenhofer, J. Molecular basis for LDL receptor recognition by PCSK9. *Proc. Natl. Acad. Sci. U.S.A.* **2008**, *105*, 1820−1825.
(64) Dray, C.; Rougon, G.; Debarbieux, F. Quantitative analysis by in vivo imaging of the dynamics of vascular and axonal networks in injured mouse spinal cord. *Proc. Natl. Acad. Sci. U.S.A.* **2009**, *106*, 9459−9464.